SANDIA REPORT

SAND97–0497 • UC–704
Unlimited Release
Printed March 1997

Characterization of the Mechanical Properties of LTCC "Green Tape"™ for the MC4352 MET

Fernando Uribe, Stephen Garrett, Saundra Monroe, Steven Burchett

Prepared by
Sandia National Laboratories
Albuquerque, New Mexico 87185 and Livermore, California 94550
for the United States Department of Energy
under Contract DE-AC04-94AL85000

Sandia National Laboratories

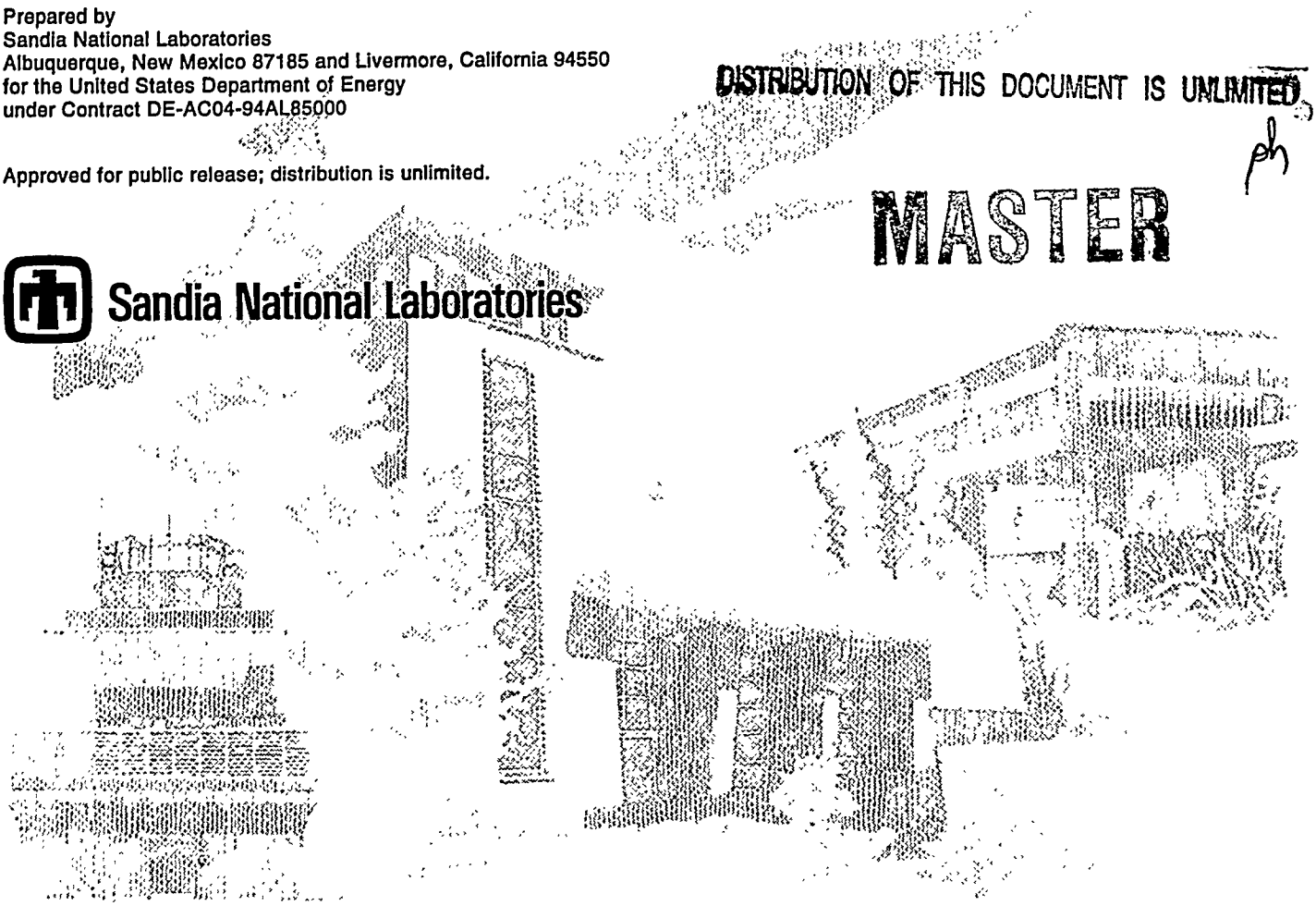

SF2900Q(8-81)

Issued by Sandia National Laboratories, operated for the United States Department of Energy by Sandia Corporation.

Available to DOE and DOE contractors from
Office of Scientific and Technical Information
P.O. Box 62
Oak Ridge, TN 37831

Prices available from (615) 576-8401, FTS 626-8401

Available to the public from
National Technical Information Service
U.S. Department of Commerce
5285 Port Royal Rd
Springfield, VA 22161

NTIS price codes
Printed copy: A04
Microfiche copy: A01

SAND97-0497
Unlimited Release
Printed March 1997

Distribution
Category UC–704

Characterization of the Mechanical Properties of LTCC "Green Tape"™ for the MC4352 MET

Fernando Uribe and Stephen Garrett
Manufacturing Technologies Center
MCM Technologies and Coatings Department

Saundra Monroe
Materials and Process Sciences Center
Materials Joining Department

Steven Burchett
Engineering Sciences Center
Engineering and Manufacturing Mechanics Department

Sandia National Laboratories
P.O. Box 5800
Albuquerque, NM 87185-0957

Abstract

During the qualification of Low Temperature Cofire Ceramic (LTCC) as an enabling WR packaging technology for manufacturing the MC4352 (MET), issues pertaining to the mechanical performance of the DuPont 951 "Green Tape™" tape were investigated. Understanding the fundamental mechanical performance of the DuPont 951 substrate material, including the effect of surface metallization in STS environments, is required to determine MC4352 survivability. Both fast fracture and slow crack growth behavior were characterized for the MET configuration. A minimum stress threshold of 6.5 Kpsi for slow crack growth was established for substrates containing surface conductors, resistors, and resistor glaze. Finite element analysis was used to optimize the MET substrate thickness and to design the supporting structures to limit mechanical loading of the populated substrate below the slow crack growth threshold. Additionally, test coupons that failed during environmental testing are discussed. The root cause of electrical failures was attributed to solder leaching of the thick film metallization. Changes to solder pad configuration were incorporated to reduce the solder-metallization intermetallic from reaching the substrate interface. Finally, four-point bend tests revealed that the YAG laser approach for sizing LTCC substrates induced flaws, which substantially reduced the overall strength of the test samples as compared to samples sized using a diamond saw.

Acknowledgments

The authors would like to thank the following people at Sandia for their contributions to this work: C. Nowlen, J. Gieske, B. Ritchey, M. Stavig, B. McKenzie, C. Newton, G. Zender, A. Kilgo, and J. Stephens. In addition, we are indebted to all the people at Allied Signal Federal Manufacturing and Technologies, Kansas City Division, who were involved in this project.

Contents

Contents *(continued)*

Figures

Figures *(continued)*

Figures *(continued)*

Tables

This page intentionally left blank

Characterization of the Mechanical Properties of LTCC "Green Tape"™ for the MC4352 MET

1. Introduction

The high interconnect density afforded by Low Temperature Cofire Ceramic (LTCC) technology makes it an attractive packaging design alternative for future weapons applications. The intended first user of this technology is the MCCS Encryption Translator (MET). Qualification/certification of LTCC packaging, as a viable WR technology, is predicated on characterization of the LTCC technology physical properties and on performance in stockpile environments. The bulk of the LTCC technology development for the MET was performed at Allied Signal Federal Manufacturing and Technologies (ASFM&T), and is documented in an internal report entitled *Qualification of Low Temperature Co-fired Ceramic (LTCC) Network Technology*. Certain aspects of the development program were performed at Sandia National Laboratories, where Sandia's technological expertise in finite element analysis, fractography, solder technologies, and LTCC packaging were utilized to characterize the mechanical properties and performance of LTCC, as well as to perform root cause analysis on test failures that occurred during the technology development cycle. Results from supporting activities performed at Sandia National Laboratories are documented in this report.

Technology characterization activities were performed on test coupons fabricated at both CTS Corporation, in West Lafayette, Indiana, and at ASFM&T, in Kansas City, Missouri. Three distinct test coupon designs were used to characterize the performance and properties of LTCC. Of primary importance for MET applications were (a) adhesion of soldered thick films to the LTCC substrate, (b) long- and short-term resistor performance, and (c) survivability at end-use environments. The coupon design used to assess survivability performance during system test requirements is referred to as a Test Vehicle (TV), and is shown in Figure 1. The TV's architecture, physical characteristics, and construction, model the design of the MET functional unit. The response variables used to assess performance of the TV coupons were mechanical integrity and electrical continuity of a daisy chain pattern routed through the six layer LTCC substrate, solder-attached leadless chip carriers (LCC), passive components, and edge clips.

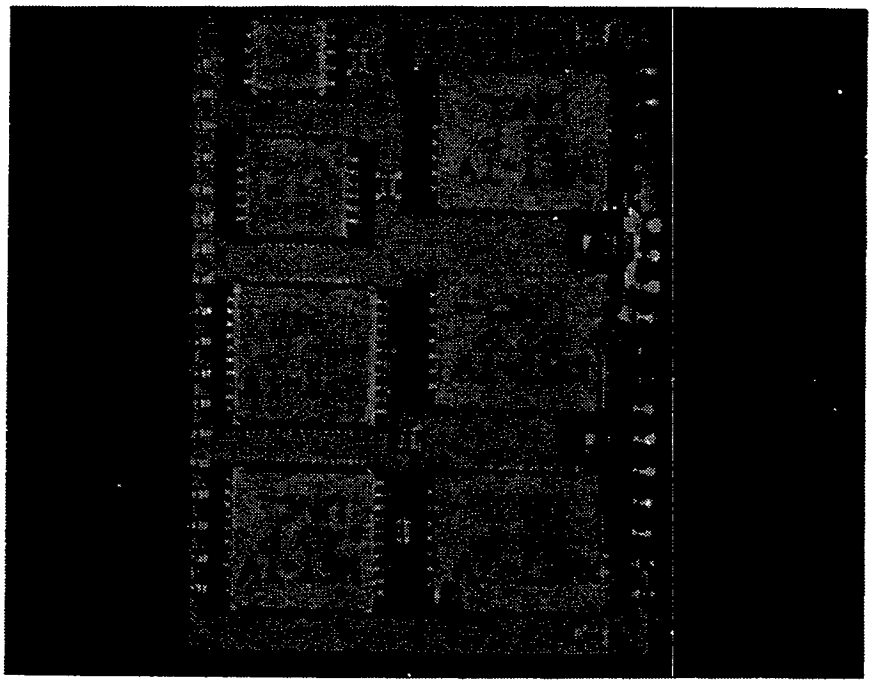

FRONT

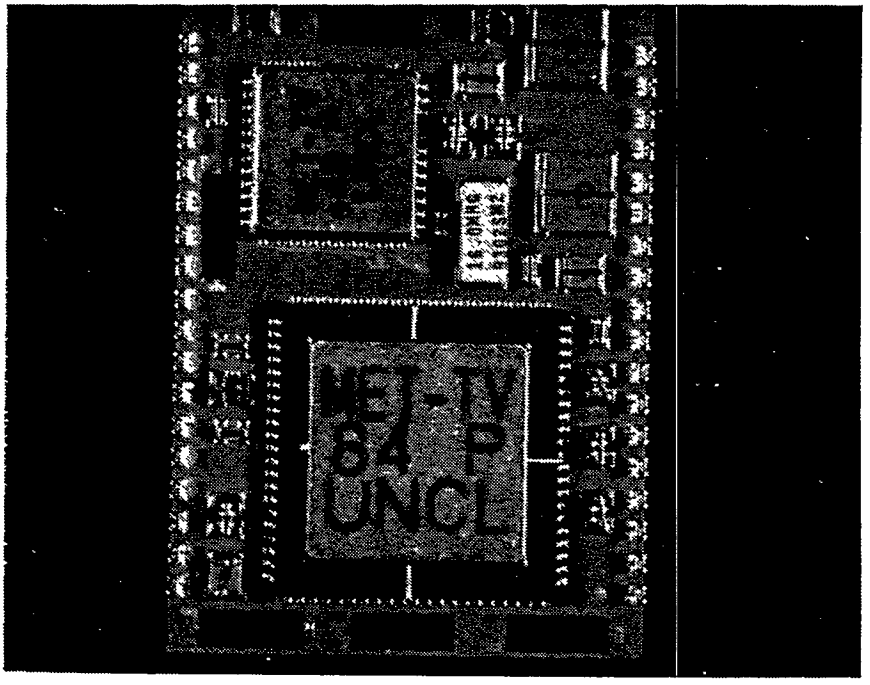

BACK

Figure 1. Front and back view of the MET populated Test Vehicle.

2. Mechanical Characterization and Finite Element Analysis Modeling

The published mechanical strength of DuPont 951 Tape, usually reported as modulus of rupture, is in the 46.4 Kpsi range, which is approximately 60% the strength of alumina. This material property is of vital concern since it could impact the ability of the MET LTCC substrate to survive the qualification test requirements, as well as program stockpile-to-target sequence (STS). As a consequence, characterization of the mechanical performance of the MET LTCC substrate, based on finite element analysis and empirical testing, was included as part of the LTCC Qualification program activities and are discussed in this section.

2.1 Slow Crack Growth Behavior

There are two important aspects to the mechanical performance of glass and ceramic materials. First is the time-independent fast-fracture behavior, generally reported as strength from modulus of rupture tests. Second is the time-dependent behavior, which is controlled by environmentally assisted subcritical crack growth (SCCG), also referred to as stress corrosion cracking or slow crack growth. SCCG is common to many glasses and ceramics, including alumina, and in many glasses[1] there is evidence that a threshold exists below which no crack growth can occur. Understanding the contribution that both of these mechanisms play in the mechanical behavior of a glass or ceramic is necessary when assessing how a material will perform during stockpile lifetime. Of equal importance is determining both the residual and functional stresses when evaluating the suitability of a material for a specific application.

Early in the qualification program, the SCCG susceptibility of the DuPont 951 Green Tape system was brought to the attention of the qualification team from data made available by DuPont. Sub-critical crack growth occurs because chemical bonds in a glass or ceramic at the tip of a flaw become more susceptible to rupture when stress is applied in the presence of certain environments, typically moisture. This behavior occurs at stress levels well below the values measured in typical strength tests. The flaws can extend subcritically as long as the driving forces — stress plus environment — are present. The stresses that drive flaw extension can be from (1) residual stresses due to mismatch in the coefficient of thermal contraction (CTC) of the materials that are bonded together, (2) stress induced by thermal cycling, and/or (3) stress developed by mechanical loading from handling, processing, or other environmental exposure.

Studies by DuPont, to investigate the SCCG behavior of the 951 tape, were conducted on post-fired test bars in which a diamond indent was introduced. There were no internal features such as conductor traces or vias in the test bars. The bars were broken in a 4-point bend test at different stressing rates. In addition to establishing that the 951 material was susceptible to SCCG behavior, a crack growth threshold of 8.7 Kpsi (60 MPa) was determined.

A preliminary study was undertaken at Sandia to determine if some of the processing required to fabricate a functional MET LTCC substrate (metallization, dielectric coatings, and trimmed resistors) would influence the strength and SCCG behavior. Some of the possible effects attributed to processing include, but are not limited to, (1) the production of sufficient stress to drive SCCG, (2) the alteration of the chemistry in the LTCC to change its susceptibility to SCCG, and (3) the introduction of very large flaws that would cause catastrophic failure at lower than anticipated stress levels. The study was not ideal because all aspects of the processing could not be included. However, the results of the study, in combination with FEA modeling and extensive test vehicle environmental evaluation performed at ASFM&T, would provide the necessary information to assess the viability of LTCC technology for the MET.

2.1.1 Test Procedure

The mechanical evaluation was performed on 30 test vehicles manufactured by CTS using DuPont 951 LTCC material. While the test vehicle sample geometry was not ideal for a four-point bend test, it was the only structure available to test the areas of interest. The coupon dimensions were 1.5 inches wide by 2 inches long and consisted of 8 tape layers yielding a total fired thickness of .030 inches. The test coupon architecture simulated the functional MET substrate design, including DuPont 4596 surface metallization, laser-trimmed DuPont 1900 series resistors with DuPont 9137 overglaze.

The coupons were tested at ambient temperature (75°F) and 15% to 30% relative humidity conditions in a four-point bend configuration. The majority of samples were supported over a 1.57-inch (40-mm) span and loaded over a .78-inch (20-mm) span at constant stressing rates. Figure 2 shows the uniformly stressed area. There were 3 to 4 replicates at each stressing rate with the back surface containing the thick film resistor network placed in tension; this was identified as Group A. A few samples (Group B) were tested using a different support and span to evaluate fixturing effects. Four samples, comprising Group C, were tested with the front surface in tension using only one fast and one slow stressing rate to evaluate strength where no resistors were present. Finally four .050-inch-thick substrates (Group D), fabricated at ASFM&T with no resistors or laser trim processing, were tested at one high stressing rate. Failure origins were identified on each test specimen.

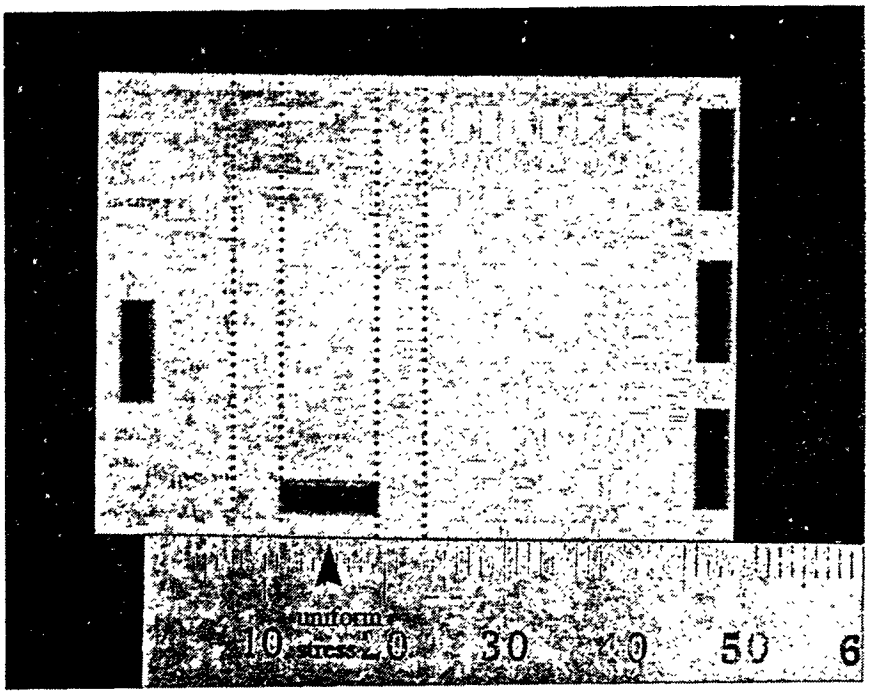

Figure 2. MET, non-populated substrate, tested using 4-point bend test conditions, ambient humidity and temperature.

2.1.2 Results

Results from testing are plotted in Figure 3. At high stressing rates, the measured strength of the .030-inch-thick substrates, Group A samples, was 12.5 Kpsi (85 MPa), and as the stressing rate decreased, the strength decreased to 6.5 Kpsi for all stressing rates below 1 MPa/sec. In test Groups B and C, the curves are shifted to a higher value of failure strength for a given stressing rate. The fast fracture strength of group D, the .050-inch-thick substrates, was 16 Kpsi (113 MPa). Fractographic analysis for each of the substrates, summarized in Table 1, revealed that failure origins were different from group to group.

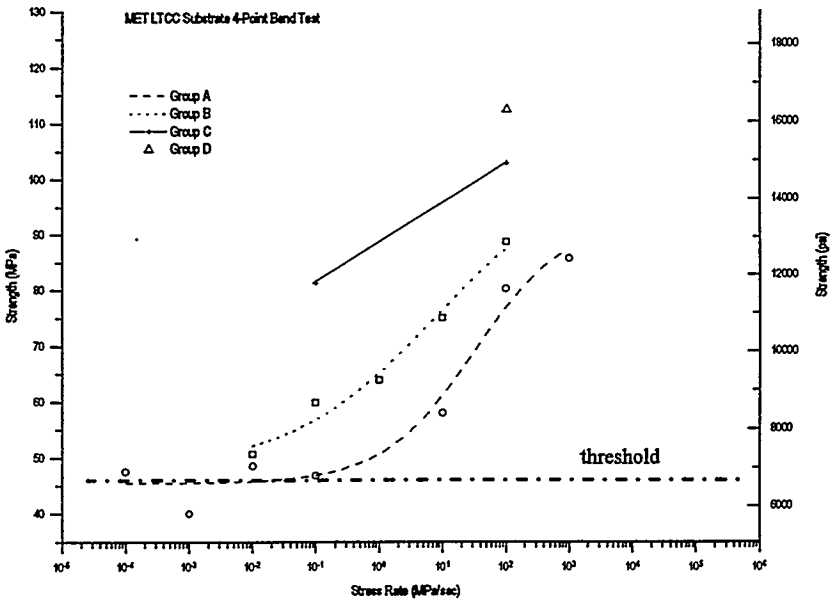

Figure 3. Threshold stress measured on non-populated MET substrates.

Table 1. Fractographic Analyses.

Group ID	Failure Origin Locations			
	Resistor	4596 Metallization	Vias	Intrinsic
A and B	17	5		
C		1		3
D			4	

2.1.3 Discussion

The results of these tests confirm the anticipated SCCG behavior of the 951 LTCC substrate material. Slow stressing rates allow the environment, particularly moisture, sufficient time to reach the crack tip and initiate subcritical crack growth. Final failure occurs once the crack has reached a critical size. The shape of the Group A curve in Figure 3 is similar to that reported by DuPont. The strength decreases with decreasing stressing rate and a SCCG threshold plateau is defined. The threshold plateau, below which SCCG does not occur, is 2.2 Kpsi lower in the Group A than that reported by DuPont for unmetallized 951 material. Failure origins for the A and B group were generally at the 4596 conductor/resistor/glaze interface.

These results show that the presence of metallization slightly reduces the SCCG threshold plateau in 951 LTCC. The higher plateau strength reported for Group B suggests there is a small effect of fixturing on the test. Group C samples failed from intrinsic defects in the LTCC and from the LTCC/4596 metallization interface. These data indicate that Group C defects were smaller than the resistor flaw origin location in Groups A and B. Group D fast fracture strength was higher than the other groups. Nominally, groups C and D should have been the same because the processing was equivalent; however, the apparent difference could be within the error of the measurement. A larger number of samples would have to be tested to establish statistically relevant differences between groups C and D.

2.1.4 Conclusions

This preliminary study shows that SCCG behavior and the threshold value reported by DuPont were not dramatically changed once 4596 metallization, resistors, resistor glaze, and resistor laser trim were incorporated in the 951 tape. The series of tests revealed that the metallization/resistor/glaze interface was the primary location of failure origin, but if residual and static stresses remain below the 6.5 Kpsi threshold, no SCCG is expected. FEA analyses, reported in Section 2.3, of the most severe loading condition (142-G shock level) for the MET in a normal transportation environment, shows that when the new design for the MET is incorporated (.050-inch-thick substrate and center support), a maximum stress of 2.5 Kpsi will develop. The 142-G shock level test is a transient condition that simulates a potential environment encountered during transportation. Also considered were the long-term static stresses present, which are attributed to the differences in TCE's between the soldered components and the LTCC substrate (see Section 3.4) where no evidence of subcritical crack growth was observed. These data indicate that the total stress is below the SCCG threshold, and no crack growth is expected, which would degrade the mechanical performance of the MET.

2.2 Strength Study of Saw-Cut and Laser-Scribed LTCC Substrates

2.2.1 Background

Mechanical tests were performed on DuPont 951 LTCC substrate material to compare the effect of diamond saw cutting versus laser scribing on strength. As a benchmark, Coors, ADS-96R 96% alumina thick film substrate material was also tested. A four-point bend test geometry was used for the mechanical evaluation.

Laser scribing/breaking and saw cutting are methods used to size substrates for microelectronics applications. Both methods introduce some damage into the edges of the substrate, and depending on the extent of the damage, can affect the mechanical performance of the substrate. Since the MET has both shock and vibration requirements,

where reduced substrate strength could cause failure, any operation that introduces damage must be evaluated for its effect on mechanical performance. Both diamond sawing and YAG laser scribing were evaluated for sizing of LTCC substrate for the PPI build of the MC4352 (MET).

The YAG laser has traditionally been used to scribe and size alumina substrates at ASFM&T. Due to production time constraints, laser parameters were not systematically evaluated and optimized for processing LTCC material. Therefore, this study only examines the effect of a single set of YAG laser processing parameters on the strength of DuPont 951 LTCC substrate material. The intent of this evaluation was not to determine the optimal laser processing parameters for laser scribing LTCC, but rather to evaluate the differences in damage introduced by these operations, and the potential impact this could have on the strength of the test bars.

A YAG laser, referenced at ASFM&T as Holobeam (Control laser), was used to scribe the LTCC and alumina test bars. LTCC material was laser scribed using full power output (7 to 10 watts), a 0.3-in/sec feed rate, and a 5KHz pulse rate. After laser scribing, bars were fractured to complete the bar separation. A Microautomation 1006 wafer saw was used to cut both LTCC and alumina bars. The saw was equipped with a resinoid blade, and water was used as coolant. A .015-inch-deep cut per pass was made on both LTCC and alumina. These two sample preparation processes introduce typical laser damage and saw cutting damage into the test bars along the long axis, which is placed in tension during the four-point bend test. Nominal LTCC bar dimensions were .048 inches thick by .250 inches wide and 1.5 inches long. Nominal alumina bar dimensions were .040 inches thick by .250 inches wide and 2 inches long. All samples were made and processed at ASFM&T and sent to SNL for testing.

2.2.2 Test Parameters of ASFM&T Samples

A four-point bend test was used for the mechanical evaluation based on a standard ASTM test method[2] but the load and support spans were slightly modified. This procedure places the laser-scribed and saw-cut edges of the test bars in tension during the mechanical test. The four-point bend testing geometry used to test the bars is shown in Figure 4. A 1.02-inch supporting span and 0.32-inch load span were used in testing, with a loading rate of .02 inch/minute in air, and relative humidity ranged from 30-35%. The sample and load support dimensions do not exactly follow the ASTM method for four-point bend testing but were selected to allow testing of as many bars as possible. LTCC and alumina bars were separated into three groups: saw cut, laser-scribed entry side, and laser-scribed exit side. Saw-cut test samples were obtained from ASFM&T and DuPont using their standard processes. The DuPont saw-cut samples were not available for testing at the same time as the ASFM&T prepared samples. Results of tests on ASFM&T saw-cut and laser-scribed samples are reported in Sections 2.2.2 through 2.2.6. Results of the DuPont saw-cut samples are reported in Section 2.2.7.

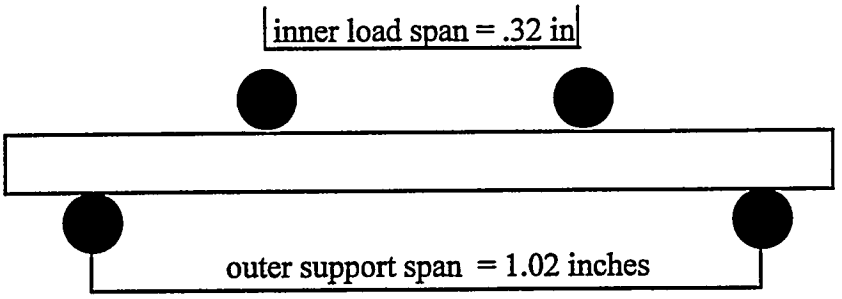

Figure 4. Four-point bend sample and loading configuration.

2.2.3 Optical Examination

All test bars were examined optically before and after testing. The original test definition included three groups (laser exit, laser entry, saw cut), but optical examination of the LTCC bars before testing revealed some large chips on some of the saw-cut surfaces. This newly defined set of bars (saw-cut, most damage) was grouped for data reduction. Another optical observation was that the LTCC laser-scribed bars did not have a smooth planar fracture beneath the scribe line. The edge surface was not perpendicular to the top surface, and it deviated out of plane. The four-point bend test geometry assumes a uniform cross-section to be tested, so each laser-scribed LTCC bar was marked to load as uniform a cross-sectional area as possible. An implication of the non-planar appearance of this edge is that the laser did not introduce the correct scribe to get a uniform break in the LTCC material. The saw-cut LTCC bars had not been completely parted during the saw-cutting operation, leaving a small tail on one side of the bar. This tail was removed by chamfering the edge with 320 grit SiC grinding paper, and that edge was placed on the compressive side during the mechanical test. A complete saw cut, during production, is essential in order to correlate the mechanical test data in this study with expected mechanical performance of production parts. Laser-scribed and saw-cut alumina bars had no chips or tails on edges.

After testing, the fracture surface of each bar was examined optically to determine the location of the failure origin. In fact, not all bars broke from the saw-cut or laser-scribed edge, but rather some bars broke from a defect along the width of the bar. For data analysis purposes, "mid-bar" breaks were defined as another group. Bars that broke from a mid-bar defect (pore, large grain, inclusion, inhomogeneity, etc.) can be considered as representing the "intrinsic" material strength.

2.2.4 Mechanical Strength Test Results

Failure strength (σ_f) was calculated using the following equation:

$$\sigma_f = 3P(L_o - L_i) / 2bh^2$$

where: P = failure load, L_o= support span, L_i = load span, "b" and "h" are sample width and thickness, respectively. Table 2 contains the calculated strength from the four-point bend testing for all groups evaluated. Table 3, contains test results after fracture surfaces were examined. Specific failure origins were identified, and where appropriate, bars were assigned to "mid-bar" break groups. The identification of the "mid-bar" break group allowed determination of an "intrinsic" failure strength of these materials. The data reported in Sections 2.2.4.1 and 2.2.4.2 refer to data in Table 3, where additional strength information was obtained by determining the actual failure origins and grouping the bars on that basis.

Table 2. Summary of all data.

Material	Process ASFM&T	Tensile Surface	Number Samples	Avg. Strength (Ksi)	Std. Dev. (Ksi)
LTCC	saw cut	all	39	32.3	5.0
LTCC	laser scribe	entry	23	18.7	2.2
LTCC	laser scribe	exit	21	33.7	4.8
Alumina	saw cut	all	14	60.6	5.0
Alumina	laser scribe	entry	15	53.3	5.8
Alumina	laser scribe	exit	14	58.3	4.4
	DuPont				
LTCC	saw cut	all	25	27.3	5.2
Alumina	saw cut	all	30	53.9	6.8

Table 3. Summary of grouping by failure location.

Group ID	Material	Process	Tensile Surface	Number Samples	Average Strength (Ksi)	Std. Dev. (Ksi)
a	LTCC - corner break	saw cut	less damage	22	32.4	5.2
b	LTCC - corner break	saw cut	most damage	4	32.1	5.4
a/b	LTCC mid-bar break	saw cut	less/most	13	32.1	5.0
c	LTCC - corner break	laser scribe	laser entry	23	18.7	2.2
d	LTCC - corner break	laser scribe	laser exit	4	36.1	3.3
d	LTCC mid-bar break	laser scribe	laser exit	17	33.1	5.0
a'	Alumina - corner break	saw cut	less damage	5	58.4	7.9
a'	Alumina mid-bar break	saw cut	less damage	9	61.8	3.6
e	Alumina - corner break	laser scribe	laser entry	15	53.3	5.8
f	Alumina - corner break	laser scribe	laser exit	14	58.3	4.4
			total	126		

2.2.4.1 LTCC Test Results

Failure strength, calculated from saw-cut LTCC samples, is 32.3 Kpsi, regardless of observed damage level differences. Failure strength of laser-scribed bars with the laser exit side placed in tension is 36.1 Kpsi. Laser-scribed test bars, where the laser-entry side was placed in tension, failed at 18.7 Kpsi. This represents a 40% reduction in strength, which is significant when compared to all other LTCC groups. There is no significant difference in the strength of bars (32 to 33 Kpsi) where the fracture originated at the mid-bar location, regardless of saw-cut or laser-scribe processing.

2.2.4.2 Alumina Test Results

Overall failure strength of the saw-cut 96% alumina was 58.4 Kpsi. Intrinsic failure strength, as estimated by "mid-bar" failures, was 61.8 Kpsi. Laser-exit-damaged bar strength is 58.3 Kpsi and laser-entry-damaged bar strength is 53.3 Kpsi. The laser-entry damage reduces the strength of the alumina bars by 11%.

2.2.5 Discussion

Defects (flaws) introduced in the process of laser scribing reduced the strength of both the 951 DuPont LTCC substrate and the benchmark material, 96% thick film alumina. The large population of bars tested in this study provides confidence that the statistical distribution of flaw size has been captured. Strength is a direct function of the flaw size in a material as defined in the following equation:[3]

$$\sigma_f = K_{IC} / Yc^{1/2}$$

where:
σ_f = failure stress, Y= a geometric factor, K_{IC} = fracture toughness (a constant material property), and c=flaw size. Larger flaws, introduced by the laser-scribe process, substantially reduce the strength of the LTCC substrates.

2.2.6 Fractographic Analysis

SEM micrographs of the failure origins in the laser-scribed LTCC and alumina are shown in Figures 5 and 6. The laser-damage zones are shown in Figure 5 and failure origins in Figure 6. Clearly the damaged zone is more extensive in the LTCC material than in the alumina, extending 90 microns versus 65 microns respectively, into the depth of the substrate surfaces. Also the remelted zone in the LTCC appears well attached to the substrate as compared to the damaged zone in the alumina, which appears to have spalled off in some locations.

The more adherent nature of the damaged zone in the LTCC may explain why the strength degradation in the LTCC was greater, 40%, compared to only 11% observed in the alumina. Examination of the failure origins in representative LTCC and alumina bars shows the damaged zone in the LTCC was clearly responsible for the failure. In the alumina bar that is not so clear. The fracture origin is located at the corner, but the flaw size appears to be smaller than the zone affected by the laser process.

2.2.7 Mechanical Test Results of DuPont Saw-Cut Samples

The DuPont saw-cut samples were mechanically tested using the same fixtures and testing condition used for the ASFM&T saw-cut samples. The average strength measured on the DuPont saw-cut LTCC was 27.3 Kpsi with a standard deviation of 5.2. The average strength measured on the DuPont saw-cut 96% alumina was 53.9 Kpsi, with a standard deviation of 6.8. As in the ASFM&T saw-cut samples, examination of the bend bar fracture surface showed that not all failures occurred at the corner of the bars. Many were located mid-bar, indicating that the saw-cutting operation did not introduce excessive damage to the substrate. The DuPont prepared sample average strength is slightly less than the ASFM&T saw-cut test bars. The difference is within the standard deviation of the measurement. Small differences in the measured value may be attributed to subtle difference such as fixture alignment or variability in relative humidity.

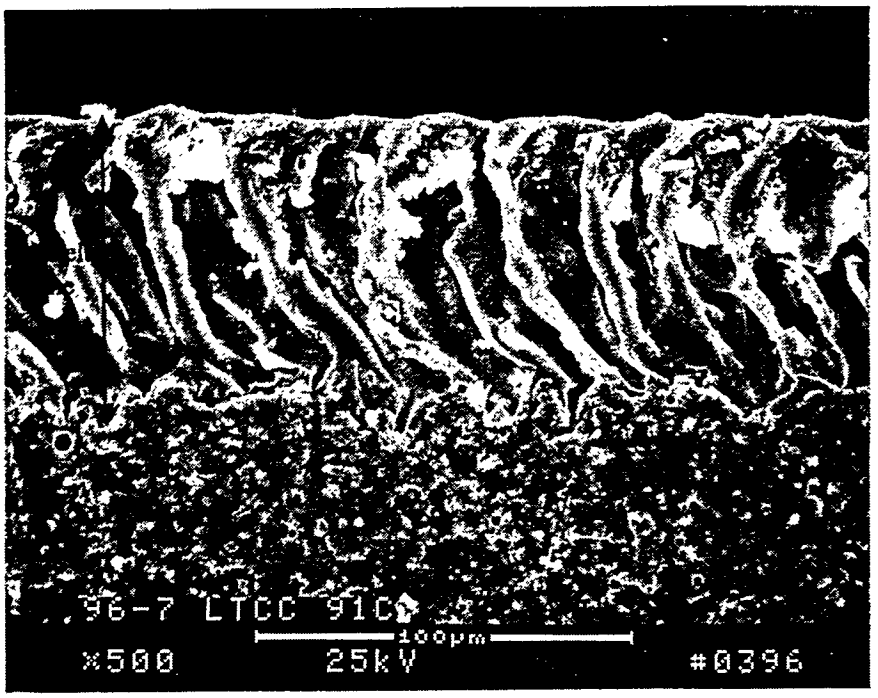

A

B

Figure 5. Laser entry side of bend bars shows remelt damage zone where failure originated.

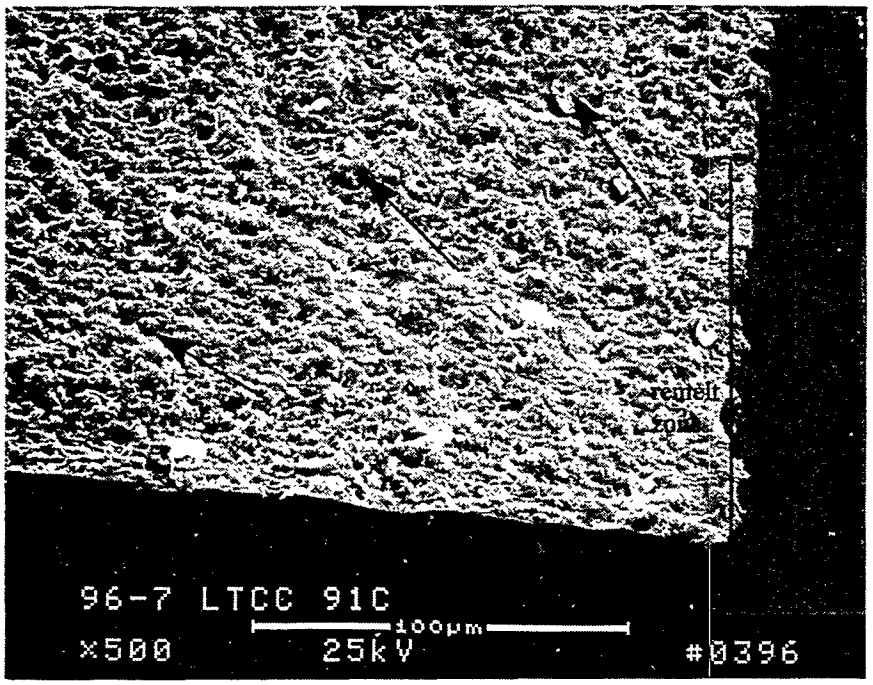

A

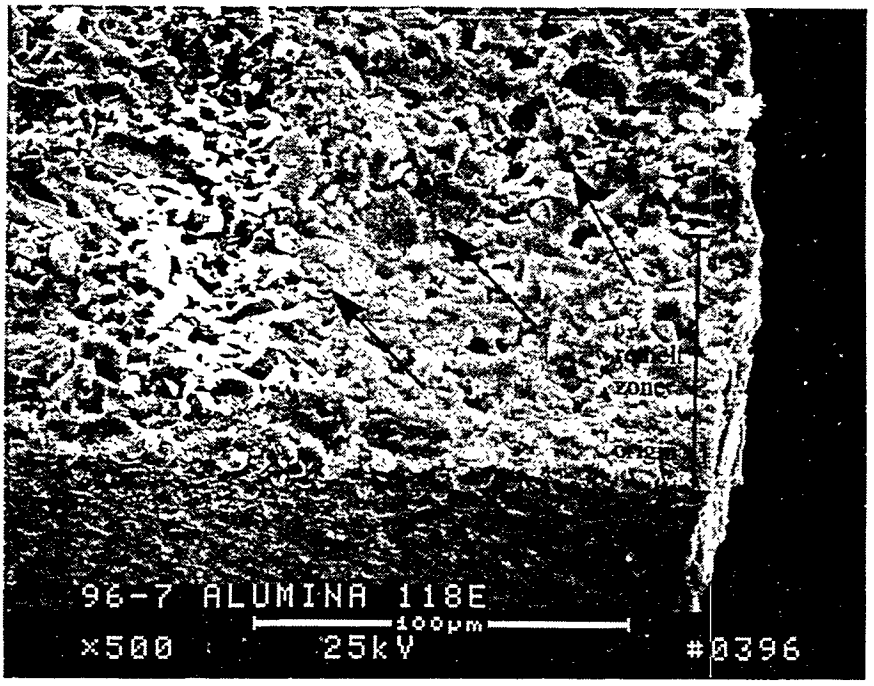

B

Figure 6. Fracture surface shows failure origin and remelt zone at origin.

2.2.8 Conclusions

The average strength measured on the bench mark DuPont saw-cut LTCC and alumina samples is not substantially different from the measurements made on the ASFM&T saw-cut samples. The flaws introduced in the saw-cut and laser-scribed exit surfaces appear to be similar in size and the failure strengths are equivalent, 32 Kpsi and 33 Kpsi respectively. Most significant is the strength reduction observed in both alumina and LTCC when the laser entry surface is placed in tension. The reduced strength indicates that flaws introduced into the laser entry scribed surface of both LTCC and alumina are larger than the intrinsic flaws normally found in the fired material or flaws introduced by the saw-cutting operation.

2.3 Computational Studies in Support of the MCCS Encryption Translator (MET)

2.3.1 Introduction

In support of MET design activities, computational finite element studies to estimate (1) the fundamental natural frequency of the MET substrate and (2) the peak computed stress in the substrate for a 142-G, 6.5-ms applied shock load were completed. Four design configurations (0.040-inch and 0.050-inch-thick substrates both with and without center foam center support) were evaluated. The results from these studies were then used to perform a preliminary evaluation of a proposed shock watch device to be used during shipping of MET devices. This section summarizes the results of the computational evaluation.

2.3.2 Model Description

The finite element idealization for a 0.050-inch-thick substrate with a center foam support is shown in Figure 7. In this model, the LCC components were modeled as solid blocks, however, the density of the blocks was varied to reflect the correct weight of individual packages. The components were attached to the substrate through solder pads. Although the solder pads should satisfactorily reflect stiffness of the substrate, there is insufficient mesh density in the solder to accurately compute stresses (in the solder). Fixed boundary conditions were applied to the upper and lower surfaces of the corner and center foam supports. The assumed mechanical properties of the materials in the assembly are given in Table 4.

This page intentionally left blank

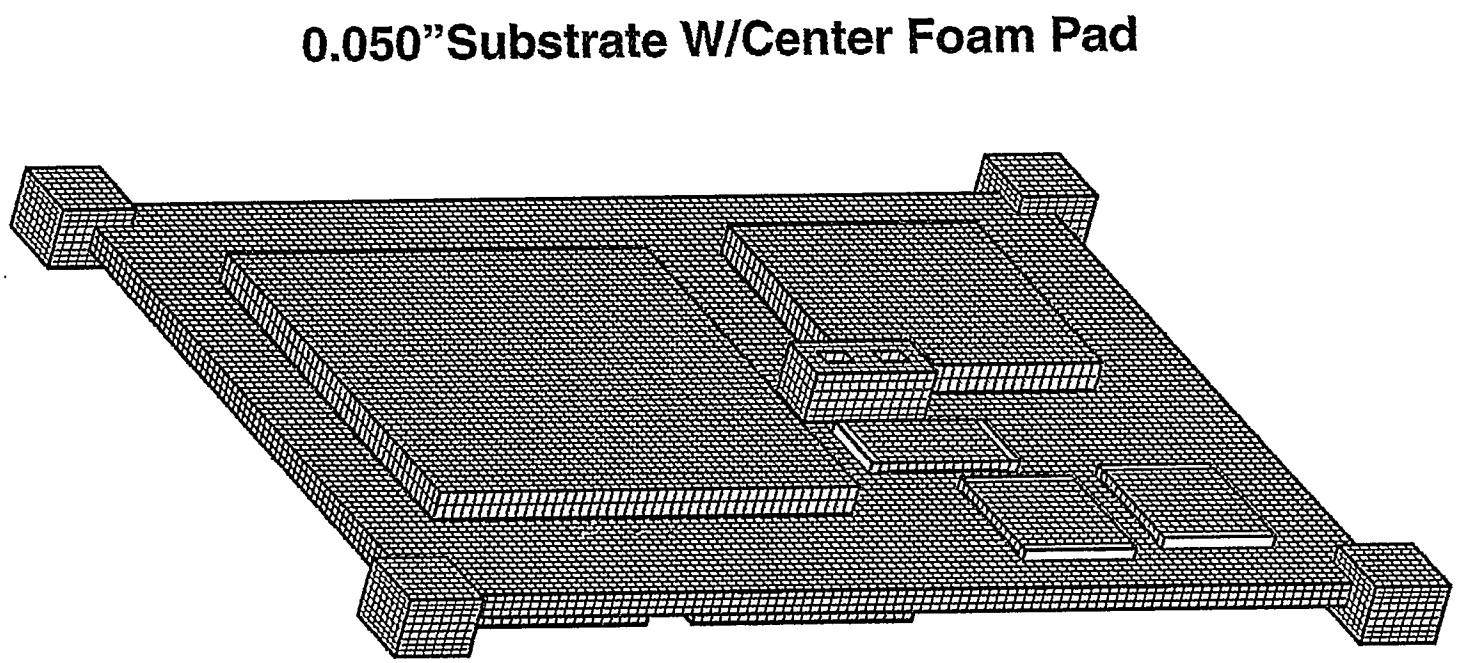

Figure 7. Finite Element Idealization

This page intentionally left blank

Table 4. Material Properties.

Material	Youngs Modulus (psi)	Poissons Ratio	Comments
LTCC Substrate	18.74E+6	0.232	
LCC Components	40.0E+6	0.17	Density varied to reflect weight of components
Solder	2.0E+6	0.4	
Foam	7872.0	0.45	
Resistor Components	40.0E+6	0.17	Density varied to reflect weight of components

All materials were assumed to respond linearly elastic and to be temperature independent. The stress-strain response of the foam pads are actually nonlinear; however, an average linear elastic modulus was chosen. The assumed modulus of the foam reflects a linearized portion of the stress-strain curve corresponding to the precompression set. The initial height of the pads were 0.2 inch and the compressed height was 0.115 inch.

2.3.3 Results

2.3.3.1 Fundamental Frequency

The fundamental frequency of the MET assembly was computed using the general purpose finite element code ABAQUS. The results of this study, given in Table 5 indicate that increasing the substrate thickness from 0.040 inch to 0.050 inch slightly increases the fundamental frequency. The addition of the center foam pad support, however, substantially increases the fundamental frequency. Having this frequency above 2000 cps is desirable to minimize coupling with high-energy shock loads.

Table 5. MET Substrate Evaluation — Fundamental Frequency.

Substrate Definition	Fundamental Frequency (cps)
0.040-inch Substrate WO/Center Pad	1061
0.050-inch Substrate WO/Center Pad	1202
0.040-inch Substrate W/Center Pad	2620
0.050-inch Substrate W/Center Pad	2740

2.3.3.2 Stress Due to Applied Shock Load

The stress in the MET substrate assembly for an applied constant acceleration load in both the +Z and -Z direction was computed using the general purpose finite element code ABAQUS. The shock load of most concern (142 G's @ 6.5 ms) is of sufficient duration that the acceleration can be considered to be applied statically. In Figure 8, contours of the computed maximum principal stress in the assembly for the applied acceleration load in the -Z direction (tending to bow the substrate up) are plotted. The peak stresses in the substrate are summarized in Table 6. These results indicate that the computed peak stresses are sufficiently below the slow crack growth threshold of 6500 psi even for the 0.040-inch-thick substrates.

2.3.4 Shock Watch Evaluation

During shipping of the MET device, a shock watch monitor is intended to be used. The purpose of the monitor is to determine if the MET was subjected to potentially damaging shocks during shipping environments. A preliminary evaluation to determine the usefulness of the shock watch was completed. From shock testing of the MET device, it was determined that a 0.050-inch substrate with a center foam support can withstand a shock test of 1000 G's, 2.5 ms but fail a shock test of 1250 G's, 2.0 ms.

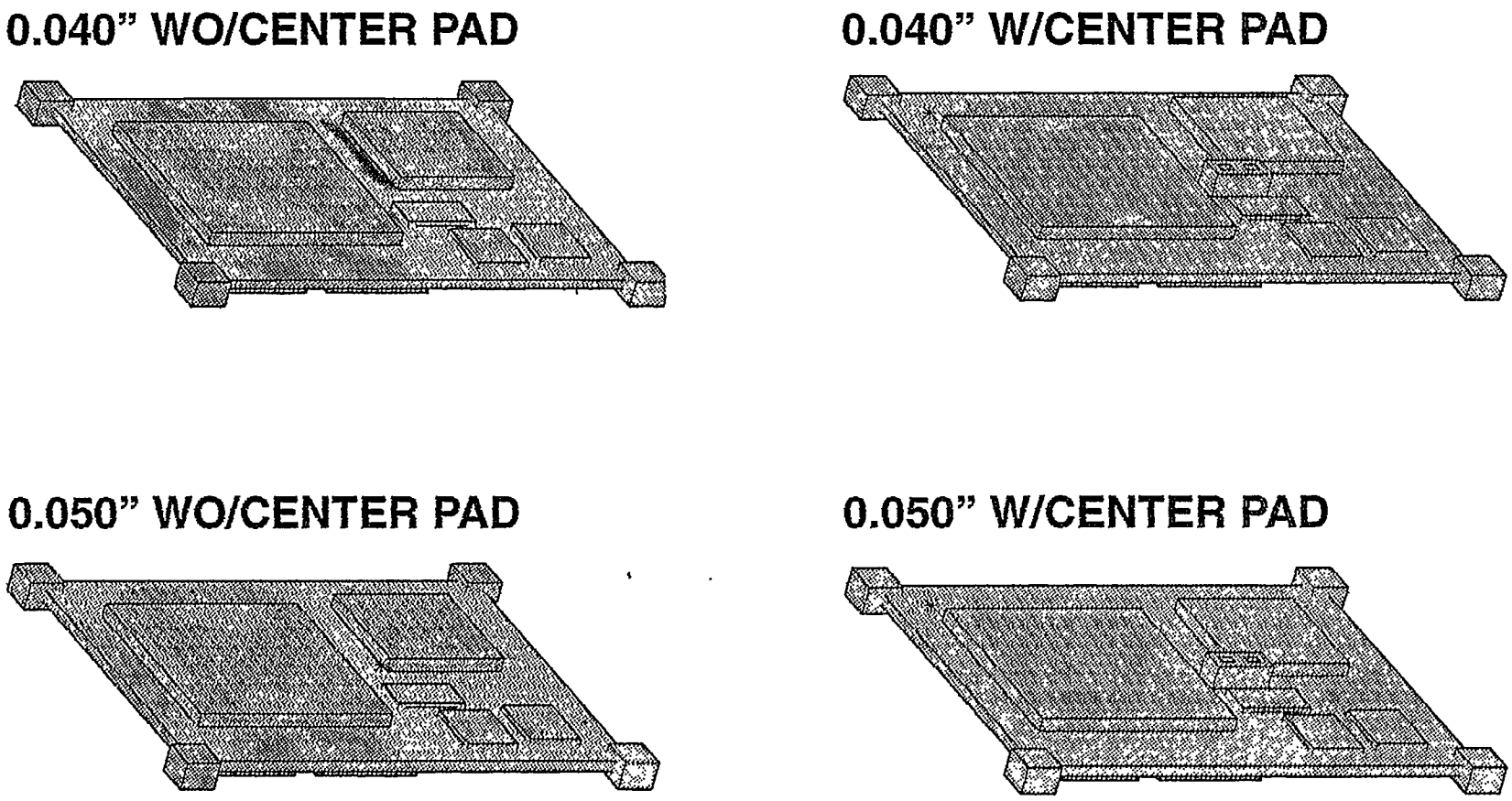

Figure 8. Computed Maximum Principal Stress in Assembly Due to Acceleration Load

This page intentionally left blank

Table 6. MET Substrate Evaluation — Stress Due to Acceleration Load in the +/– Z Direction.

Substrate Definition	Maximum Stress 142 G (psi)	Maximum Stress per G (psi/G)
0.040-inch Substrate WO/Center Pad	5177	36.46
0.050-inch Substrate WO/Center Pad	4299	30.27
0.040-inch Substrate W/Center Pad	2919	20.55
0.050-inch Substrate W/Center Pad	2519	17.74

Using these values, the failure stress in the LTCC substrate was computed (from the previous section) to be between 17,750 - 22,175 psi. These values are consistent with strength values for LTCC ceramic. The shock watch has four shock level indicators corresponding to 128 G @ 6.5 ms, 381.5 G @ 1 ms, 681.5 G @ 0.5 ms, and 3100 G @ 0.1 ms. Table 7 presents the evaluation of the shock watch monitor as applied to the MET device. The amplification factor was obtained from response spectra assuming that the fundamental frequency for the substrate was 2742 cps.

The results of this evaluation suggest that failures in a MET device with a foam center supported 0.050-inch substrate could occur before the shock watch triggers for the 681.5 G @ 0.5 ms and the 3100.0 G @ 0.1 ms shock levels. The computed stress level in the substrate for the 381.5 G @ 1.0 ms shock is approximately equal to the measured slow crack growth threshold of 6500 psi implying that some crack growth could occur in the substrate at this shock level.

Table 7. Shock Watch Evaluation.

Shock Watch Trigger (G's @ ms)	Amplification	Applied Acceleration (G)	Computed Stress (psi)	Failure Stress (psi)
128 @ 6.5	1.0	128	2,270	17,750 - 22,175
381.5 @ 1.0	1.0	381.5	6,767	17,750 - 22,175
681.5 @ 0.5	~1.5	1,022	18,130	17,750 - 22,175
3,100 @ 0.1	~1.0	3,100	55,000	17,750 - 22,175

This page intentionally left blank

3. Failure Analysis

An important aspect of the Qualification Program was analysis of test coupons that failed during environmental testing. Examination of failed test coupons, based on fractography, was performed to identify the failure causing problem and to determine if the failure(s) resulted from a design deficiency or a materials deficiency.

During development activities at ASFM&T, several MET TV (test vehicle) substrates were provided for analysis of fractures that occurred in the LTCC during exposure to shock, vibration, and thermal cycling test environments per the MC4352 Product Specification. The evaluation performed includes fracture origin identification, as well as a discussion of how and why the fracture occurred and whether the failure stress is consistent with what is predicted by FEA.

In addition, this section contains analyses of two substrates that were not fractured, one exposed to solder reflow only and one that was fully processed and exposed to thermal cycling. These two substrates were provided to assess whether small cracks are generally present in the LTCC where the LCC packages are soldered to the substrate. The history and evaluation of each substrate is discussed.

The methodology used to evaluate all fractured LTCC substrates includes low magnification (10 - 30×) optical examination of the macroscopic fracture pattern, followed by systematic disassembly to expose the fracture surface of each crack. The exposed fracture surfaces were further examined using higher magnification (30 - 200×) optical microscopy or SEM (scanning electron microscopy). Macroscopic and microscopic fracture features provide key information to identify the fracture origin, calculate failure stress, determine direction of crack propagation, assess potential of time-dependent failure mechanism such as slow crack growth, and evaluate how the failure stress was applied (mechanical or thermal). This information, in conjunction with FEA models of the MET, aid in determining if fracture was predictable or unexpected. In addition, weaknesses, due to processing or design, can be identified and perhaps modified. Information obtained from the fractographic analyses is documented in photo micrographs.

3.1 Test Vehicle #8

3.1.1 History

TV #8 substrate, tested at ASFM&T, was 0.040 inches thick and made using DuPont 951 material for the LTCC Qualification program. It was visually and electrically inspected before and after exposure to mechanical shock environments. TV #8 was exposed to, and passed the normal transportation shock requirement of, 142 G, 6.5 ms, and the overtest environment of a 400 G-level in + and − x, y, and z directions. It was exposed to the +/− x and +/− y directions at the 600-G level and passed, but failed

electrical testing after exposure to the + z direction at the 600-G level. The "+ z" direction for applied shock means that the front surface, containing the 7 LCC packages, was in tension. After failure at the 600-G level the part was sent to SNL for fractographic evaluation.

3.1.2 Fractographic Analysis

Figure 9A shows the substrate after exposure to the 600-G level shock test. Cracks in the substrate are clearly present at all four corners of the substrate. Higher magnification examination revealed additional cracks. All cracks are sketched on the schematic shown in Figure 9B. Examination revealed all corner cracks (A, B, C, D) and cracks 1, 2, and 3 extended completely through the substrate. Cracks 4 and 5 penetrated partially through the substrate and were only detectable on the front surface.

The four corner cracks released fragments immediately and the rest of the substrate remained intact due to mechanical support at the solder connections. The fracture sequence can be partially reconstructed where cracks intersect at corner D. Crack D existed before either crack 1 or 3. The fracture sequence of the other cracks cannot be determined because no intersection occurred. It is clear that multiple independent cracks developed in TV #8, which suggests a fast fracture event as would be expected in a shock test.

The fracture surfaces of all four corners cracks and crack 1 were examined to identify the failure origins. In Figure 9B, multiple fracture origins are marked with "o" and arrows adjacent to each sketched crack show the direction of crack propagation. All fracture origins at the four corner cracks and at crack 1 had the same character. A typical fracture surface is shown in Figures 10A and 10B. Fractographic analysis revealed the following observations:

1. Fracture originated beneath a solder pad located at the corner of the LCC package on the front surface and ran through the plate thickness.

2. The fracture surface contains cantilever curl, a feature indicating that a bending load caused the failure.

3. Fracture origins are located on the substrate surface that would have been placed in tension in during the +z orientation 600-G shock test.

4. Small zones of fracture exist (Figure 10B) beneath the solder pads, which served as the failure origins for the catastrophic fracture during the 600-G level shock test.

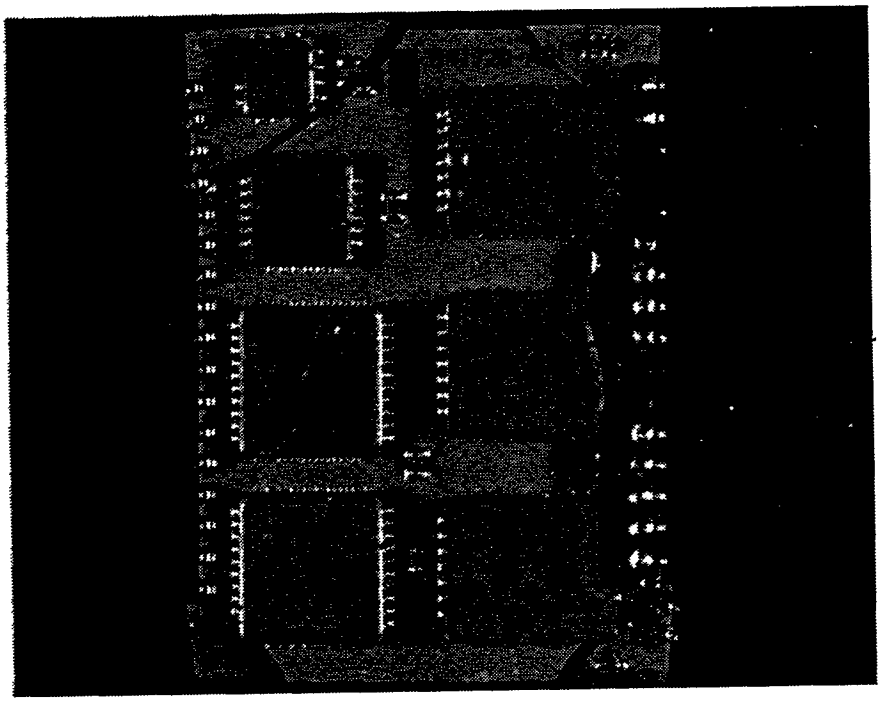

Figure 9A. TV#8, front surface after fracture during 600-G level shock overtest.

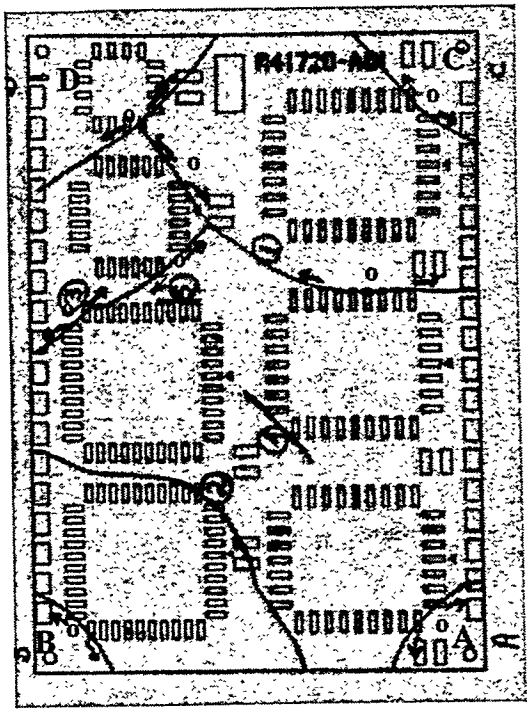

Figure 9B. Sketch of TV#8 shows all cracks observed in fractographic examination.

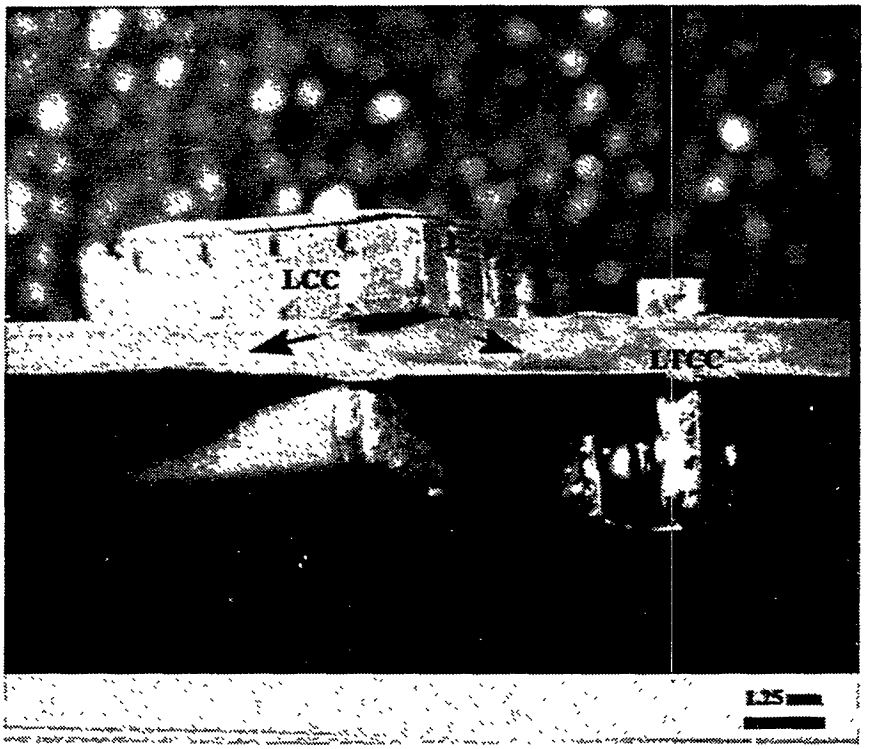

Figure 10A. Fracture surface of LTCC shows origins beneath LCC packages. Arrows indicate direction of crack propagation.

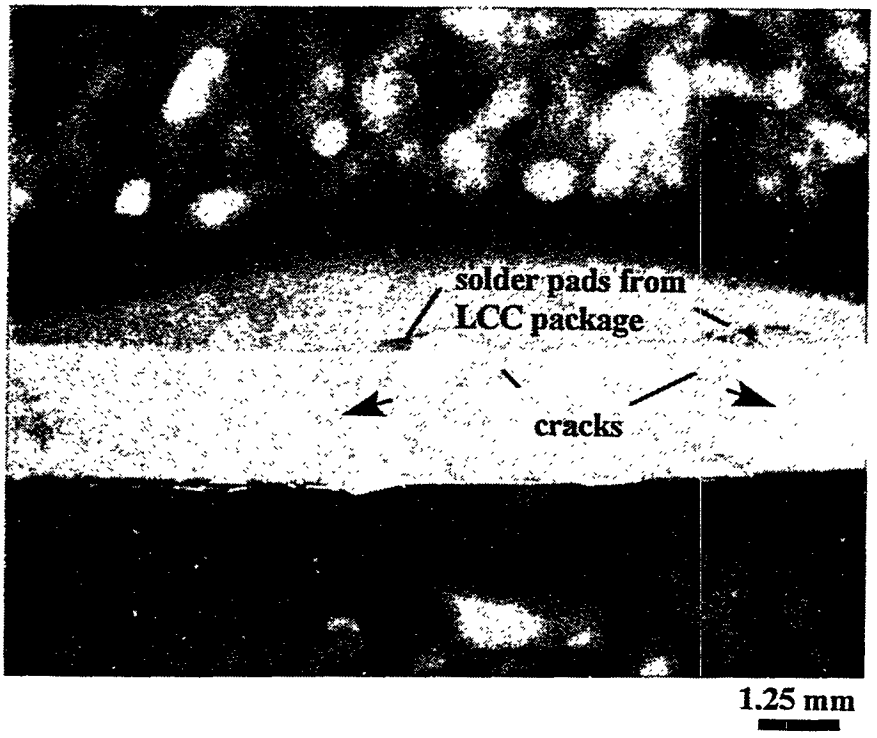

Figure 10B. Small cracks beneath LCC solder pads served as ultimate failure origins.

3.1.3 Discussion

Failure stress can be calculated from a measurement of the failure origin flaw size using the following equation,[3] where σ_f is the failure stress, K_{1C} is the fracture toughness, Y is a geometric term related to the shape of the flaw, and c is the flaw size. This relationship shows that as flaws increase in size strength will be diminished.

$$\sigma_f = K_{1C} / Y\, c^{1/2} \qquad (1)$$

Examples of flaws are shown in Figure 10B. Flaw size was measured to estimate a failure stress in TV #8 of 49.6 MPa (7.2 Kpsi). The FEA analysis of a shock-tested .040-inch-thick MET substrate with no center support, typical of TV #8, is presented in Section 2.3 of this report. That analysis estimates that a maximum of 3.6 Kpsi stress per 100 G's during shock exposure is generated at the solder joints between the LTCC and LCC packages.

The TV #8 board was subjected to increasing G-level of shock before failure finally occurred at the 600-G level. During the 142-G shock exposure, the maximum stress was estimated at 5.1 Kpsi, which is substantially below the measured 33 Kpsi fast-fracture strength of a monolithic DuPont 951 LTCC substrate material.

The next level shock exposure of TV #8 was at the 400-G level, during which a 12 Kpsi stress develops at the corner solder joints. During the 400-G level test, crack growth is possible and is potentially when the cracks shown in Figure 10B developed. Those cracks served as the final failure origins during the 600-G level shock test. At the 600-G shock level, 18.0 Kpsi stress develops, but only 7.2 Kpsi was necessary to propagate a crack from the large flaws introduced during the 400-G test.

3.1.4 Conclusions

In summary, the fracture in TV #8 was caused by the shock test. The magnitude of the stress induced by shock exposure is consistent with mechanical performance expected from the .040-inch-thick DuPont 951 LTCC substrate with no center support. There are no inconsistencies in relating the FEA modeling with observed fracture behavior of the LTCC. Ceramic materials fail when high tensile loads are applied. The observed failure origins were located on the surface of the substrate that would have been placed in tension during the shock test.

Further, the shock test would cause a bending load to be applied to the substrate, and there is evidence of fracture driven by a bending load. Fractography also shows that all failures originated at the solder joint between the corner of the LCC package and LTCC substrate. The FEA model predicts that the solder joint between the LCC and

LTCC will be subjected to maximum stress during the shock test exposure. The small zones of fracture that served as the final failure origins can be explained by prior exposure to shock levels sufficient to drive limited cracks, but insufficient for catastrophic failure.

3.2 Test Vehicle #24

3.2.1 History

Test Vehicle #24 came from the same fabrication lot as TV #8 and therefore is of the same architecture (see Section 3.1.1). It was visually and electrically inspected before exposure to thermal cycling and short- and long-term random vibration as defined in the MC4352 Product Specification. TV #24 successfully passed electrical testing at temperature extremes for all vibration tests, but upon returning to room temperature after exposure to +/– z axis of long term vibration lost electrical continuity. A large hairline crack was observed in the substrate after it was removed from the testing fixture.

3.2.2 Fractographic Analysis

Figure 11A shows TV #24 after exposure to the long-term vibration test, with a line marking the location of the single mid-plane crack. The crack extended completely through the substrate thickness. The two halves of the substrate were held together by the edge clips and kapton connector. The substrate halves were easily separated to expose both fracture surfaces. Examination of the fracture surface revealed two failure origins beneath two adjacent corner solder joints of an LCC package located on the substrate front surface.

Figure 11B shows the exposed fracture surface with an "o" placed between the two origins. The fracture surface was carbon coated to minimize internal reflection and to enhance the resolution of the crack. This micrograph clearly shows the cracks originating from the two sources and coalescing to form a very large defect. Arrest lines on the fracture surface, marked with a dashed line on the micrograph, indicate the crack propagated some distance under an applied load, stopped and at some later time propagated further.

The coalesced crack extended roughly 70% through the substrate thickness as shown by arrows in Figure 11B. This crack did not intersect any conductor line until it propagated beyond 70% of the substrate thickness. Additional examination of the fracture surface revealed cantilever curl, a fracture feature typical of failure due to a bending load.

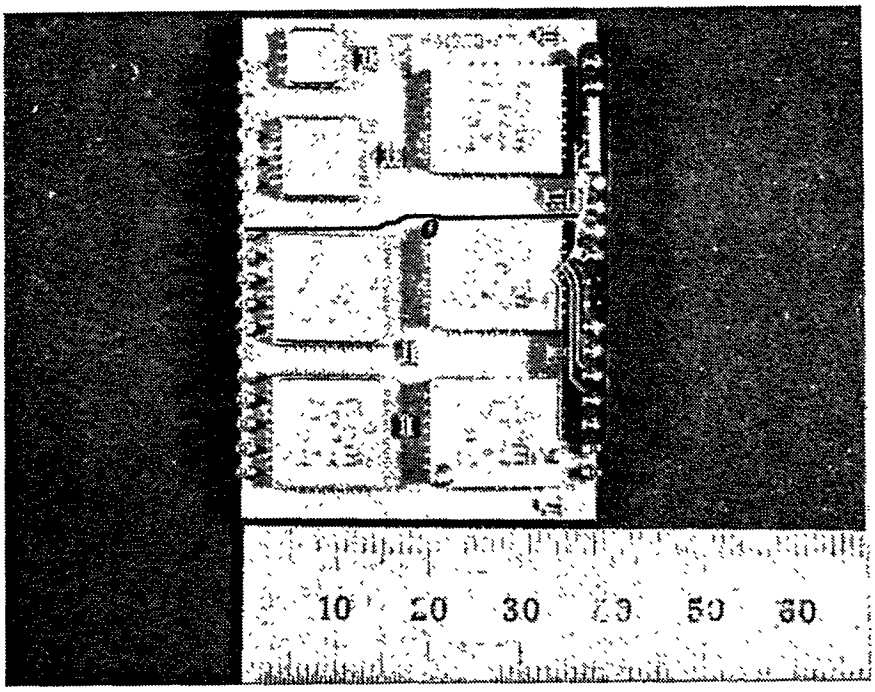

Figure 11A. A single mid-plane fracture caused failure in TV#24 after exposure to the long-term vibration environment. "o" marks the failure origin.

Figure 11B. Exposed fracture surface of TV #24 shows two bright areas on either side of "o". These small cracks extended to the position marked with a dashed line. The final failure, during long-term vibration testing, probably initiated from this very large defect.

3.2.3 Discussion

The specific conditions of the short- and long-term vibration testing are expected to produce very little load and should be insufficient to fracture a LTCC substrate. This assumes that a uniform distribution of flaws exists in the surface of the substrate. However, as was shown in Equation 1 (Section 3.1.3) in the analysis of TV #8, the presence of a very large flaw allows cracks to propagate at loads considerably lower than expected from typical strength data. The fractographic examination of TV #24 revealed large failure origins (flaws) that are not typical of the normal population of flaws in the LTCC material. The large flaws are located beneath the solder pads, which was identified by FEA modeling (Section 2.3) as a high-stress location under a bending load.

The most logical hypothesis to explain how TV #24 survived the short-term vibration and failed in the subsequent long-term vibration is that the large origination flaws were present in the MET before short-term vibration testing. The flaws were probably introduced during handling, in the form of a bending load. The load was sufficient to cause a small amount of crack propagation. While these cracks are large from a failure defect perspective, they would not have been detected electrically because they did not intersect any internal conductors and, due to overlaying solder pads, were obscured from optical identification.

The possibility exists that these cracks extended to the coalesced dimension as a result of exposure to short-term vibration. This level of loading was sufficient for crack extension, but not to produce a catastrophic failure. In this state, TV #24 substrate was very susceptible to fracture when exposed to even a very benign mechanical loading environment like the long term vibration. In summary, evidence suggests a large defect was introduced into TV #24 as a result of handling, which was ultimately responsible for catastrophic fracture from the benign mechanical loads introduced during the vibration testing.

3.3 Serial Numbers #2 and #3

3.3.1 History

Serial numbers #2 and #3 test vehicles were fabricated by ASFM&T for the LTCC Qualification program, using the new design version of the MET. This included using six 10-mil unfired tape layers of DuPont 951 LTCC substrate, yielding a post-fired thickness of 0.050 inch; the substrate was supported at the four corners and in the center. Serial Numbers #2 and #3 were exposed to incremental increases of shock levels in the + and - z axis of 600 G/4.0 ms, 800 G/3.0 ms, and 1000 G/2.5 ms. Both substrates fractured when exposed to the 1250-G, 2.0-ms shock level. The cracked substrates were provided for fractographic analysis.

3.3.2 Fractographic Analysis

Figures 12A and 12B show both substrates after exposure to the 1250-G level shock test. Cracks in the substrate are clearly present at all four corners of the LTCC substrate and across the mid-plane. Examination of the failure origins at the corner cracks showed that all cracks, A, B, C, and D, originated from beneath the solder pads at the corner of the LCC packages, and are very similar to those observed in TV #8.

Mid-plane fractures, labeled E in both substrates, were more complex. In SN #2, crack E originated in two locations: one origin was observed beneath solder pads of a front surface LCC package, and the other origin was beneath the bottom surface solder pad of the crystal oscillator. The cracks from these two origins ran toward each other. Crack E in SN #3 also had two fracture origins: one at an LCC package on the front surface and one on the back surface at a capacitor solder pad. Figure 12C contains a typical corner crack with the failure origin indicated with an "o." This micrograph shows evidence of some crack extension, marked with the back of arrows, before the final fracture event.

3.3.3 Discussion

Fractographic evidence shows clearly that mechanical loads caused fracture of both substrates. The character of the fracture is like that found in TV #8 with failure originating from the front surface beneath the LCC solder pads. It should be mentioned that the survivable shock level was higher in the new design. The new design allowed SN #2 and SN #3 to survive the 1000-G level shock overtest exposure and failure occurred at the 1250-G level. Finite element analysis modeling (Section 2.3) of the new design predicted that stress level would be 1700 psi/100-G shock level. At the 1250-G level of shock, 21.2 Kpsi of stress develops in the substrate. This is below the 33.0 Kpsi fast-fracture stress measured on monolithic substrates. Both SN #2 and SN #3 were exposed to increasing levels of shock before final failure.

During the lower levels of shock, there was sufficient load applied to propagate small cracks that would serve as the final fracture origins. There is evidence on the fracture surfaces that the cracks propagated in at least two stages, which supports the scenario of crack extension before final failure. The fracture behavior observed in these two parts is typical of this type of mechanical loading and the observed failure origins are consistent with where the highest stresses occurred as predicted from the FEA modeling.

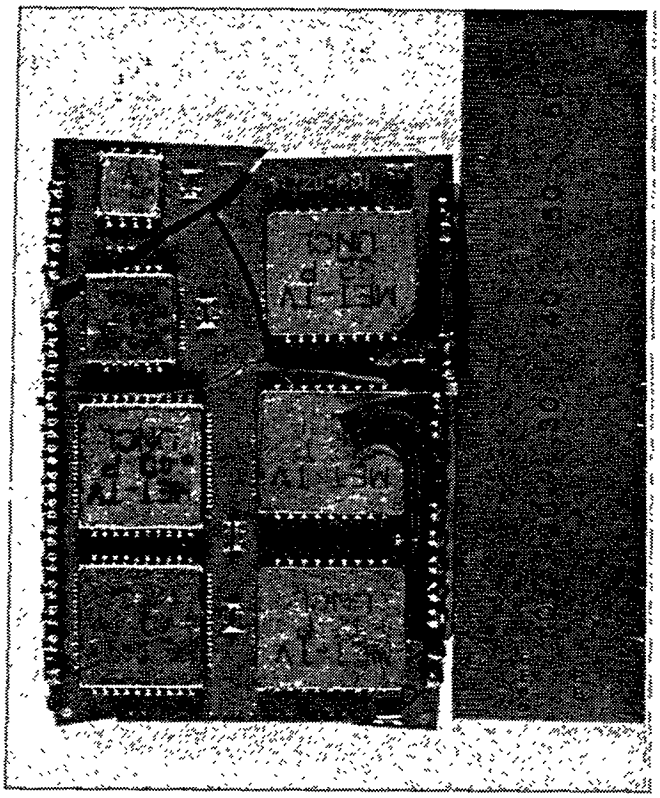

Figure 12A. S/N #2 shows fractured substrates after exposure to the 1250-G shock overtest level.

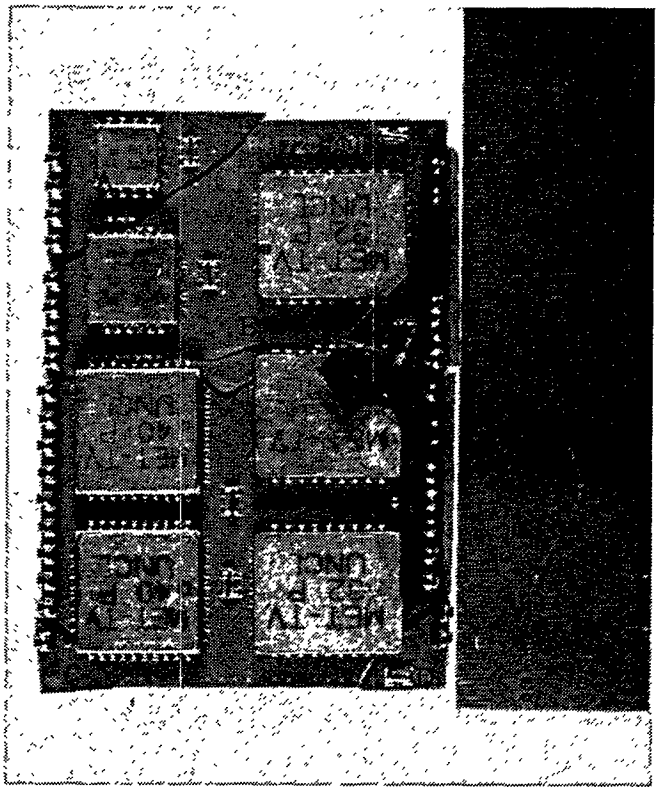

Figure 12B. S/N #3 fracture after exposure to 1250-G shock overtest level.

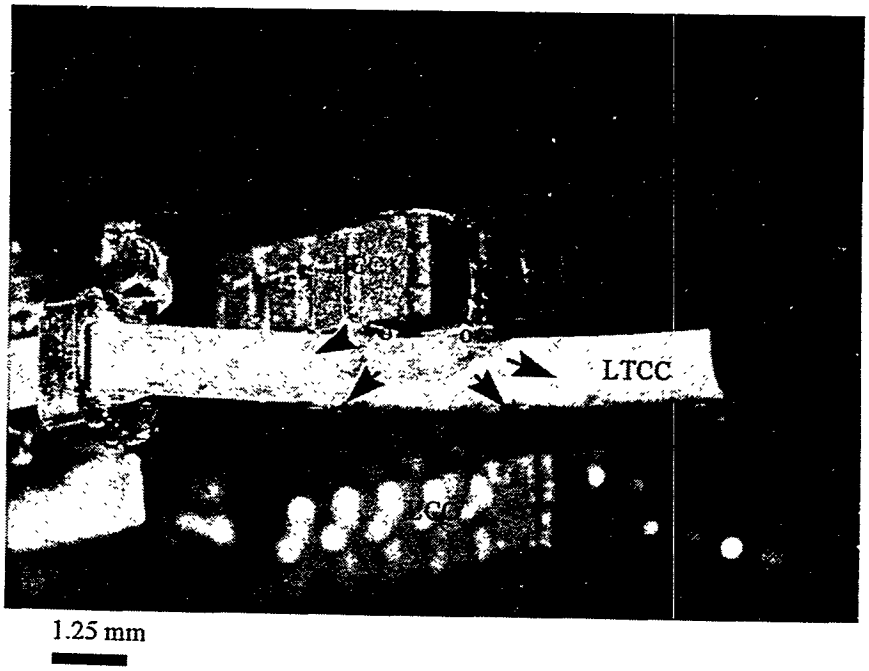

Figure 12C. Fracture surface of S/N #2, corner C, shows crack originated beneath the LCC at solder pads. The crack extended to the position indicated by the back of the arrows and propagated in the direction shown by arrow tips.

3.4 *Susceptibility of LCC Solder Pads to Subcritical Crack Growth*

Fractographic analyses of the test vehicles described in Sections 3.1 and 3.2 showed consistent failure origins located beneath the solder pads where the LCC packages are joined to the LTCC substrate. When the substrate is exposed to mechanical shock, finite element analysis modeling (see Section 2.3) showed that this is a location of high stress, due in part to residual stress.

Residual stress develops when materials with different coefficients of thermal contraction (CTC) are bonded together. In the case of the MET, the CTC of the alumina is higher than that of the LTCC substrate, and tensile stress may develop in the LTCC near the LCC/LTCC solder joint. This residual stress, if sufficiently high, has potential to drive subcritical crack growth. Additionally, the residual stress developed in the substrate can be increased when the component is exposed to thermal cycling.

Identification of the small cracks beneath the solder pads in TV # 8 and 24, which served as failure origins, raised the question of whether small cracks might be inherently present in the LTCC substrates after soldering and/or thermal cycling. Two substrates were provided for analysis: a "soldered only" substrate containing the 84-pin LCC package soldered to the back side, and a fully populated substrate, which had been subjected to thermal cycling per testing specification.

3.4.1 Fractographic Analysis

Initially, the LCC solder pad locations on both LTCC substrates were examined using vicinal illumination. There was no evidence of any cracks in the substrates. However, the small cracks observed as fracture origins in TV #8 were generally confined to the area directly beneath the solder, which would obscure their detection in a surface inspection.

The next method used to examine the "soldered only" substrate was to grind the front surface in an attempt to intersect any cracks extending from beneath the solders pads on the back surface. This method was unsuccessful. As the substrate became thinner, chipping occurred in some locations.

The final approach was to load the substrate so that the areas where solder pads were located beneath LCC packages were placed in tension. The LTCC substrate was fractured, and fracture surfaces examined. Along 50% of the perimeter of the large LCC package, on the "soldered only" substrate, the fracture occurred in the LTCC away from the solder pads. In cases where the fracture initiated at a solder pad, no evidence of small pre-existing cracks was found. This same procedure was used to examine the sample that had been subjected to thermal cycling. A sketch of the thermal cycled

substrate (Figure 13) shows 13 fracture origin locations at solder pads that were examined. A typical fracture origin in the LTCC beneath the LCC solder pad is shown in Figure 14. Again there was no evidence of any small cracks that pre-existed prior to induced fracture. The fracture surface shows uniform fracture through the thickness with no evidence that the crack may have stopped and later propagated.

3.4.2 Discussion

The procedure used in this analysis takes advantage of the fact that fracture will originate at the largest flaw. The relationship between flaw size and failure stress is discussed in Sections 2.2.5 and 3.1.3. The substrates evaluated in this section were loaded mechanically so that the area of interest was placed in tension. If small cracks existed in the LTCC beneath the solder pads, then they would serve as origins of fracture. However, no small cracks were observed. Conclusions drawn from this analysis are that insufficient stress develops in the LTCC during the soldering operation or thermal cycling to allow slow crack growth to occur in the LTCC at the solder pads beneath the LCC packages.

3.5 Test Vehicle #10

3.5.1 Environmental Exposure History of TV #10

During random vibration (short term) testing at –65°C, TV #10 exhibited an electrical open at locations indicated in Figure 15. When the part returned to room temperature, the electrical open could not be detected. Subsequent exposure of TV #10 to cold temperature once again caused the electrical discontinuity and when the sample stabilized back to room temperature, the open was still present. Prior to failure, TV #10 had been aged at 125°C for 1000 hours, subjected to random vibration (long term) at ambient, cold (–54°C) and hot (+85°C), and temperature cycled from –54°C to +85°C.

Techniques used to examine the failed unit included acoustic microscopy, optical and SEM microscopy of cross-sections, and shear testing of the leadless chip carriers. In addition to TV #10, other test coupons with different environmental conditioning history were examined. Test Vehicle #12, which had been exposed to the same environmental conditioning and mechanical testing as TV #10 but had passed all electrical testing was included in the evaluation matrix. The environmental exposure history of the TVs tested is summarized in Table 8.

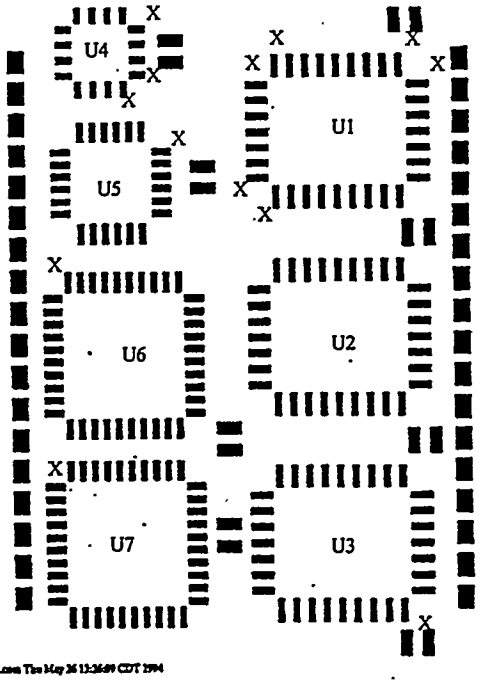

Figure 13. Schematic of locations where LCC packages are soldered to the LTCC substrate. "X" marks the location where the soldered and thermally cycled substrate was loaded in bending and fractured. The fracture surfaces at 13 locations were examined for evidence of small cracks that served as failure origins; none were found.

Figure 14. Fracture surface at corner of U4 LCC package from soldered+thermally cycled substrate. "o" marks the origin of fracture and arrows show the direction of crack propagation. No small cracks pre-existed in the intentionally fractured substrate. This is typical of all fracture surfaces examined in both the soldered only and soldered+thermally cycled substrates.

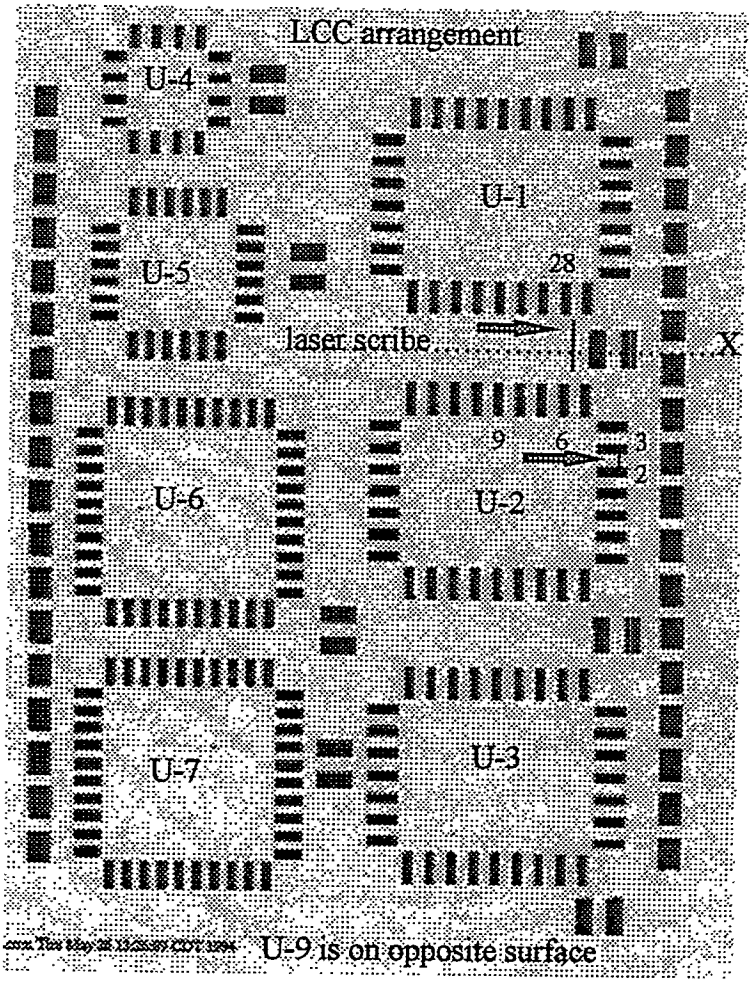

Figure 15. Schematic of front, arrows show locations of open electrical paths in TV#10.

Table 8. Environmental Exposure History of Tested TVs.

	TV #10	TV #12	TV #8	TV #8A*
AGED/SOLDERED	✓	✓		
UNAGED/SOLDERED			✓	
UNAGED/UNSOLDERED				✓

Aging: 125° C/ 1000 Hr.
Solder: 63Sn/ 37Pb
Conductor: DuPont 4596 Au-Pt
* TV #8A is a 30-mil-thick sample.
* All other samples were 40 mils thick.

The MET is a double-sided LTCC hybrid module with surface-mounted components. By design, it requires multiple printings and firings of the top Au-Pt metallization as well as multiple solder reflow operations. The Au-Pt metallization is printed, dried, and fired as one sequence. This process is repeated again to make a double-thick top metal layer, a standard process for fabricating thick film interconnect substrates, which use Au-Pt conductors for solder attach. Since both surfaces of the MET see this operation, it follows that one side will be exposed to at least four firing operations to attain double-printed metallization on both surfaces.

Initial speculation about the possible cause of failure of TV #10 centered around crack propagation through the interconnect traces internal to the LTCC substrate or delamination between the top metallization and the LTCC substrate. The crack(s) could result from subcritical crack growth due to residual stress in the package or from fast fracture during mechanical loading. Delamination between metallization and the LTCC substrate could arise from many causes such as contamination, improperly fired metallization, development of an intermetallic compound, etc.

The solder operation requires multiple reflow operations to mount all the components on both sides of the LTCC substrate. Multiple reflows of the solder provide opportunity for additional reactivity between the Au in the DuPont 4596 Au-Pt conductor and the Sn from the Sn/Pb solder. Stephens, et. al.[4] have documented that intermetallic formation can occur during a solder operation. They also showed that substantial intermetallic formation is expected to develop between the Au-Pt metallization and Sn/Pb solder at aging temperatures of 125°C for 1000 hours.

While their work was done using a 96% alumina substrate, we expect that the reactivity between the solder and metallization should be similar regardless of substrate material. They found that the thickness of the intermetallic layer is directly related to time at temperature. Intermetallics are known to be brittle in nature, may introduce stress at a joint, and potentially lead to interface separation.

3.5.2 Acoustic Microscopy Analysis

Since TV #10 was the only qualification sample exhibiting an electrical failure, it was desirable to examine this part carefully so that additional damage was not introduced. Examination using optical microscopy revealed no cracks that intersected the LTCC substrate surface. The inspection was limited to areas of the LTCC where leadless chip carrier (LCC) packages were not soldered, which severely restricted how much area could be examined.

Ultrasonic microscopy and analysis are often used as a nondestructive technique for imaging cracks and delaminations. The area around and between two LCC pads that exhibited an open circuit (see Figure 15, LCC U-2, pins 2 and 3) was examined with a number of ultrasonic techniques. A Panametrics Multiscan/Hyscan imaging system with

a 50-MHz focused straight beam was used to analyze in the top tape layer for cracks. Possible defects and cracks in the first and second layers, around the vias, was investigated using angle and surface wave beams at frequencies from 20 to 50 MHz. Images of the interfaces between the pads and buried vias were obtained but no anomalies could be identified.

The complex geometry of the fully assembled Test Vehicle made acoustic inspection for defects in the LTCC difficult. There appeared to be no other nondestructive technique(s) that could potentially yield the type of information desired in a timely and cost-effective manner. Therefore, further analysis led to cross-sectioning TV #10 and using optical and SEM microscopy techniques to determine the failure mechanism.

3.5.3 Optical Analysis

Substrate TV #10 was scribed and separated using a YAG laser to minimize damage and contamination along the line marked X in Figure 15. This exposed the conductor line connecting two LCC packages (U-2 and U-1 at pins 6 and 28) where one of the electrical opens was observed. The LTCC substrate was carefully ground perpendicular to the plane of the substrate, toward the U-2 LCC package. This grinding process should not introduce additional fracture/damage into the substrate. Grinding was done in incremental steps toward and into the toe of the solder pad at pin 6.

Optical inspection with vicinal illumination (which creates shadows when cracks are present) was used to examine the ground/polished LTCC cross-section in four locations as material was successively removed (positions 1 through 4, Figure 16A). No cracks were observed in the cross-sectioned LTCC. Once the solder pad was intersected, optical inspection showed the LTCC and solder were not in intimate contact (cross-sectioned view of position 4, Figure 16B), suggesting a weakly bonded interface. The grinding/polishing operation was stopped because of interference with the U-2 LCC package. Since no cracks in the LTCC substrate were detected that could have interrupted the electrical continuity, and there appeared to be poor contact between the solder pad and LTCC, TV #10 was encapsulated and cross-sectioned for further examination in the SEM.

3.5.4 Compositional Analysis of Separated Surfaces

During sample preparation for SEM analysis, one of the laser scribed and separated sections of TV #10 was accidentally dropped from a desktop (about 30 inches from the floor) and the U-1 LCC (Figure 15) separated from the LTCC substrate. Visual inspection of the fracture surfaces revealed complete delamination of the DuPont 4596 Au-Pt metallization pad from the LTCC substrate (Figure 17). All of the conductor

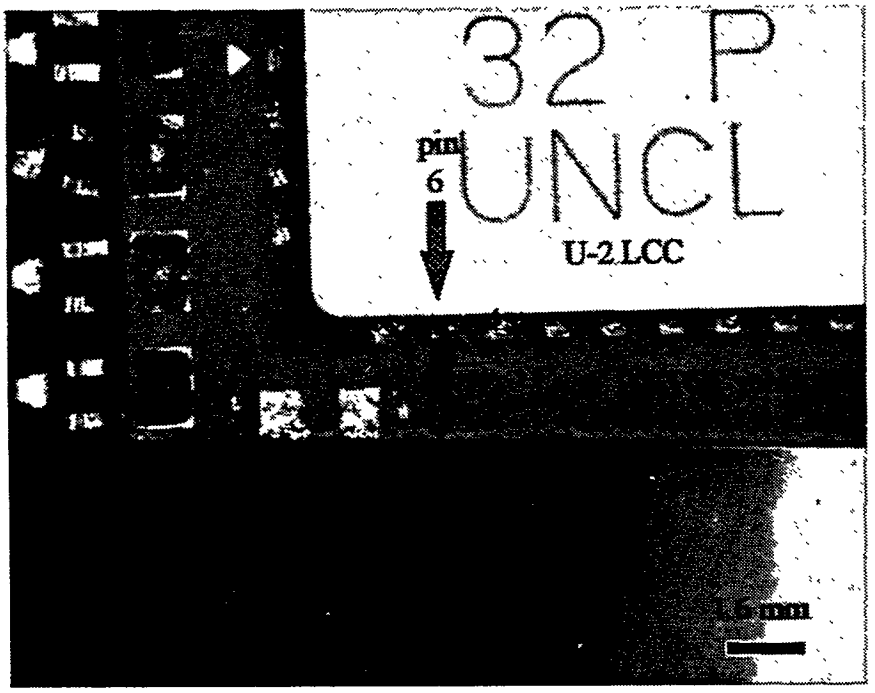

Figure 16A. Top view of MET and U-2 LCC shows locations where LTCC substrate was ground to check for cracks.

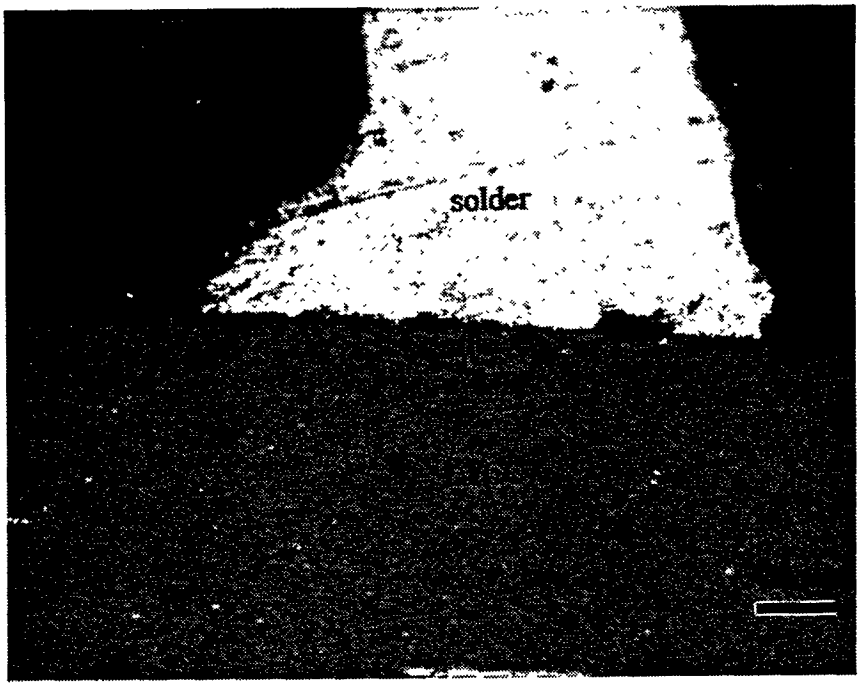

Figure 16B. Cross-section of solder joint at pin 6 shows gap between the LTCC and solder.

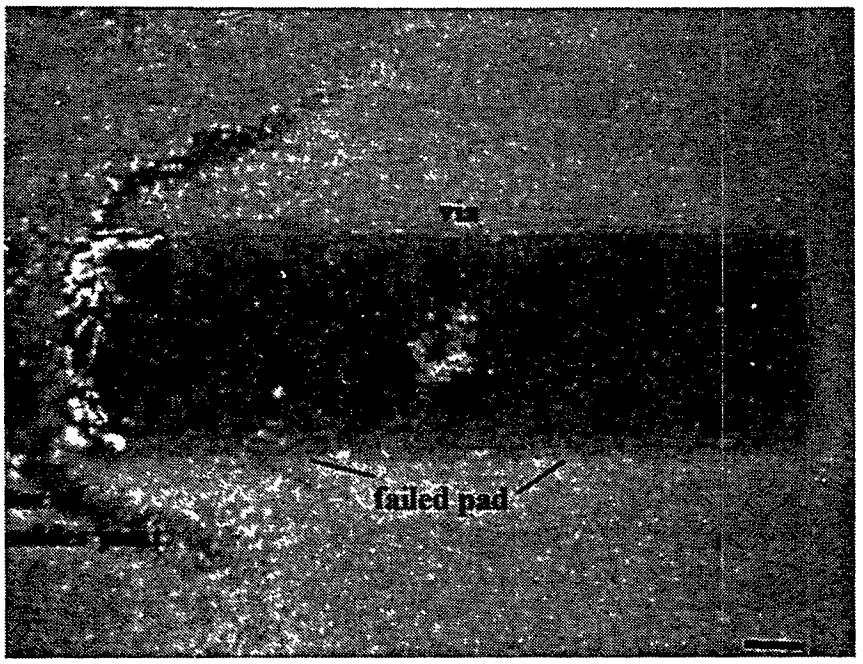

Figure 17. Low magnification view of failed pad on TV#10, U1-Pin 11. The toe of the solder joint was at the left side of the failed pad. Some thick film metal, covered by solder, can be seen at the left side of the failed pad. The gold via in the center of the pad is partially visible. Residual flux from the soldering operation is also visible in a semicircular shape to the left of the failed pad.

metallization adhered to the solder on the backside of the LCC. It was not possible to verify visually whether the original thick film metallization was present or if it had been transformed to an intermetallic compound. Energy Dispersive Spectroscopy (EDS) was performed to determine the composition at the surfaces.

EDS analysis on the backside of the LCC revealed:

1. Large amounts of Sn, which would indicate that the Pb/Sn solder had reacted with the Au-Pt thick film metallization to form an intermetallic compound at the LTCC substrate/thick film metallization interface.

2. The Sn was more heavily concentrated around the edges of the metallization rather than the center (see Figure 18). This might indicate that the Sn is migrating from the lateral (the edges of the LCC pad) directions as well as vertically (the top of the LCC pad).

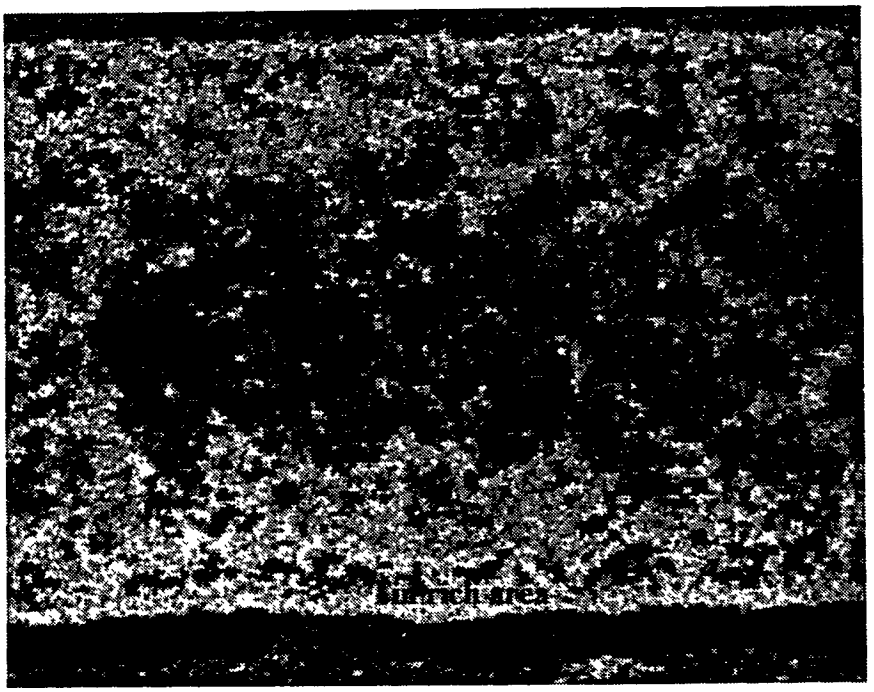

Figure 18. Compositional dot map of metallization on a backside pad of the U1 LCC from TV#10. Areas where the element tin is present are represented by the bright areas in the photo. As can be seen, the tin is more heavily concentrated around the edges than in the center of the pad.

EDS analysis on the surface of the LTCC revealed:

1. Relatively small amounts of Pt and Au, which would indicate that the fracture surface was between the LTCC surface and the intermetallic compound.

2. Glass components of the thick film material, Bi, Ca, Pb & Si, were still detectable on the LTCC surface, which would be expected. The glass components are added to improve the adhesion of the thick film metal to the ceramic substrate. During the firing of the thick film material, some of the glass material from the DuPont 4596 flows into pores and/or diffuses into the top surface of the LTCC substrate thereby creating continuous "fingers" of glass, which mechanically interlock the thick film metal with the substrate.

Based on the above analysis, the suspected cause of failure in the U-1 LCC was complete transformation of the thick film metal to an intermetallic compound, which would have been accelerated by the extended aging at 125°C. This in itself may not cause the LCC to separate from the LTCC substrate but it could create a stress raiser at the interface possibly due to the volume change generated when the Pt-Au metal

changes to an intermetallic compound such as $(Au, Pt, Pd)_1 Sn_4$. The shock generated from the accidental drop was high enough to cause the actual failure.

Another possible failure mechanism that needed to be investigated was the idea that the glass components of the thick film material segregated at or below the LTCC/intermetallic compound interface during the multiple high-temperature firings required in the processing. This segregation could in effect negate the mechanical interlocking of the glass "fingers" described above. Cross-sections of aged and unaged soldered test vehicles and unsoldered/unaged test vehicles were made to determine if any segregation of the glass components had occurred and to further characterize the formation of intermetallic compound.

3.5.5 Compositional Analysis of Cross-sections

To develop a better understanding of the cause of the weakened interface in TV #10, several polished cross-section samples were prepared. The packages and their histories are summarized in Table 8.

We examined LCC packages from TV #10 (Figure 19): (a) U-2, the LCC package with the electrical open at pin 6, (b) U-9, a package mounted on the opposing surface from U-2, and (c) U-3, a package located adjacent to U-2. TV #8A is typical of MET processing, however it does not include soldering or aging. TV #8 is an example of a substrate with soldered LCC packages, but no exposure to aging environments. TV #10 and TV #12 are parts that were fully processed and exposed to the long-term aging environment, 125°C for 1000 hours. TV #10 had an electrical open after aging and TV #12 did not. These parts were selected for evaluation to provide a comparison of how processing and environmental conditioning might have changed or influenced the character of the bond interface. All cross-sections were examined in the SEM and elemental analysis was done with Energy Dispersive Spectroscopy, EDS.

The SEM analysis focused on looking for any anomalous microstructural characteristics at the DuPont 4596 Au-Pt/LTCC interface, which could have contributed to the separation in TV #10. The character of the metals (metallization and solder) and ceramic (LTCC) was examined. An ideal interface requires some interdiffusion between the glassy phases of the LTCC and the DuPont 4596, just as a liquid phase reaction is required between the solder and metal constituents of the DuPont 4596. The DuPont 4596 metallization layer contains both metallic (80 wt. %) and glass (20 wt. %) constituents that serve as a material "transition" between the ceramic LTCC substrate and the metallic solder used to attach the LCC packages.

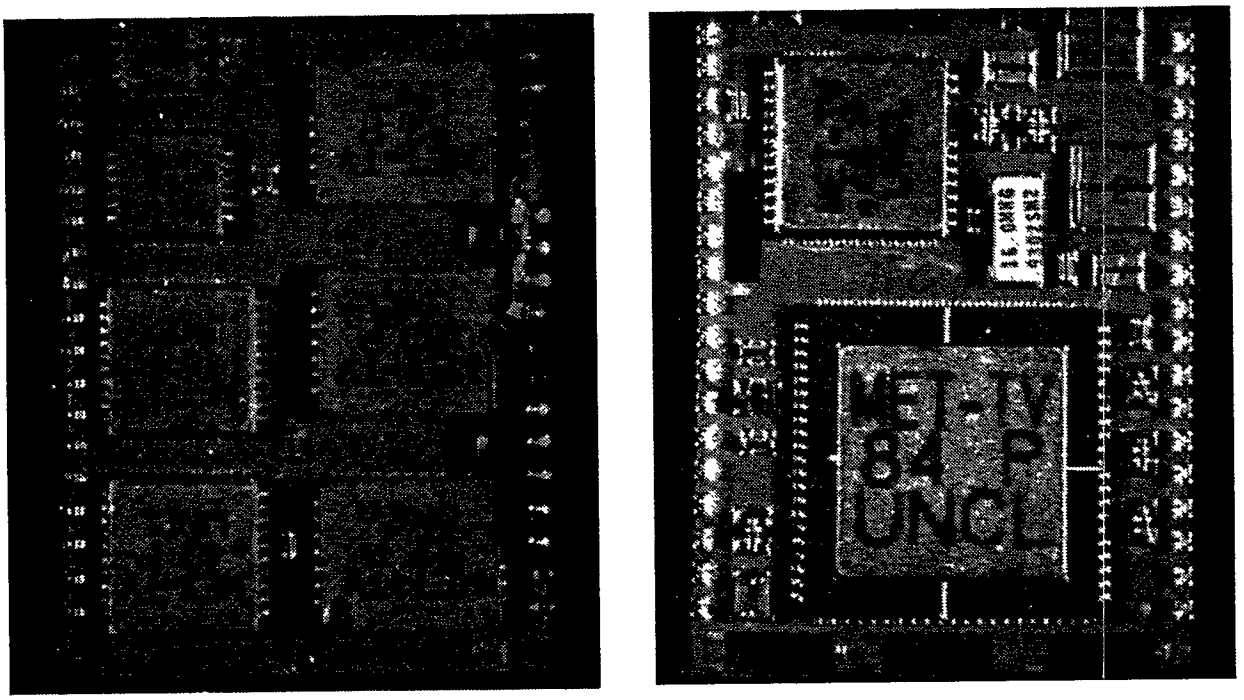

Figure 19. Front and back of MET Test Vehicle.

The thickness of the Au-Pt metallization was also measured. This thickness is critical for ensuring that a sufficient amount of metallization is still present after exposure to processing and long-term aging environments. As discussed previously, intermetallic compounds can form between Pb/Sn solder and Au metallization layers. The presence of an intermetallic layer is acceptable as long as it does not consume the entire Au-Pt metallization layer. The results of the Au-Pt conductor thickness measurements are summarized in Table 9. Micrographs and EDS analyses, that represent the typical character of the cross-sections of all substrates examined, are shown in Figures 20 through 26.

3.5.5.1 Test Vehicle #8A

Unpopulated TV #8A is a substrate that had not been exposed to any solder assembly operation or environmental conditioning. This part provides baseline information about the characteristics of the DuPont 4596 Au-Pt metallization before any solder processing and allows examination of the opposing surfaces of the LTCC, which have a different number of metallization firings. SEM micrographs of the cross-section of TV #8A are shown in Figure 20A and 20B. The low magnification image in Figure 20A shows the LTCC substrate, vias, internal conductors, and Au-Pt surface conductors.

Table 9. Thickness Comparison of Intermetallic Layers.

Part ID	Location	Treatment	Bi into LTCC (microns)	4596 Thickness (microns)	Inter-metallic Thickness (microns)
TV #8 unpop		4596 fired			
U-9 side	via midpoint		20	34	--
U-2 side	large solder pad		16	30	--
U-2 side	via midpoint		18	34	--
TV #8 unaged		4596 + solder			
U-1	long. midpoint		20	30	3-6
U-1	"		20	30	5
U-1	trans. midpoint		20	30	2-4
#12 aged, no					
U-1	long. midpoint	4596 + solder	20	islands	90
U-1	over via (solder limited supply)		20	islands	60
U-1	trans. midpoint		16	islands	90
TV #10 aged		4596 + solder			
U-2, pin 4	long. midpoint		18	islands	75
U-2, pin 6	trans. midpoint (solder limited)		20	islands	60
U-9	long. midpoint		20	islands	90
U-3	trans. midpoint		20	islands	85-100
U-2, pin?	long. midpoint		20	islands	90
U-2, pin?	long. midpoint		20	islands	90

Cross-sections were made of the conductors over vias on both the front and back surfaces of the LTCC substrate. The higher magnification micrograph in Figure 20B is typical of the DuPont 4596 microstructure in both surfaces. The image in Figure 20B, taken using SEM backscatter mode, shows contiguous porosity in the Au-Pt conduction layer and little or no porosity in the LTCC. Five different areas, shown in Figure 20B, were analyzed using EDS.

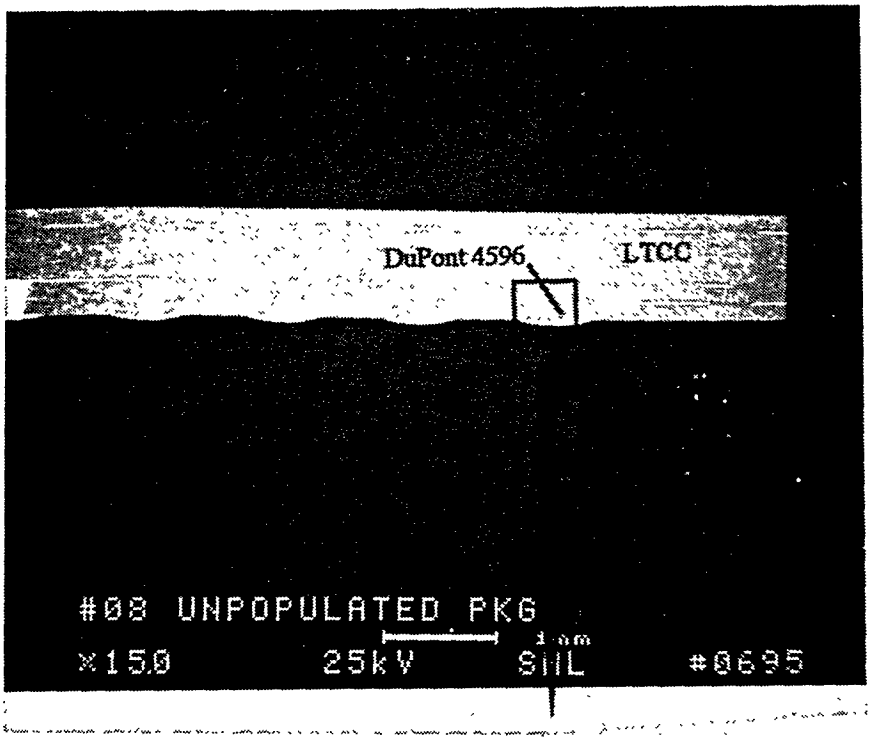

Figure 20A. Low magnification image of cross-sectioned #8A, the unsoldered, unaged MET Test Vehicle.

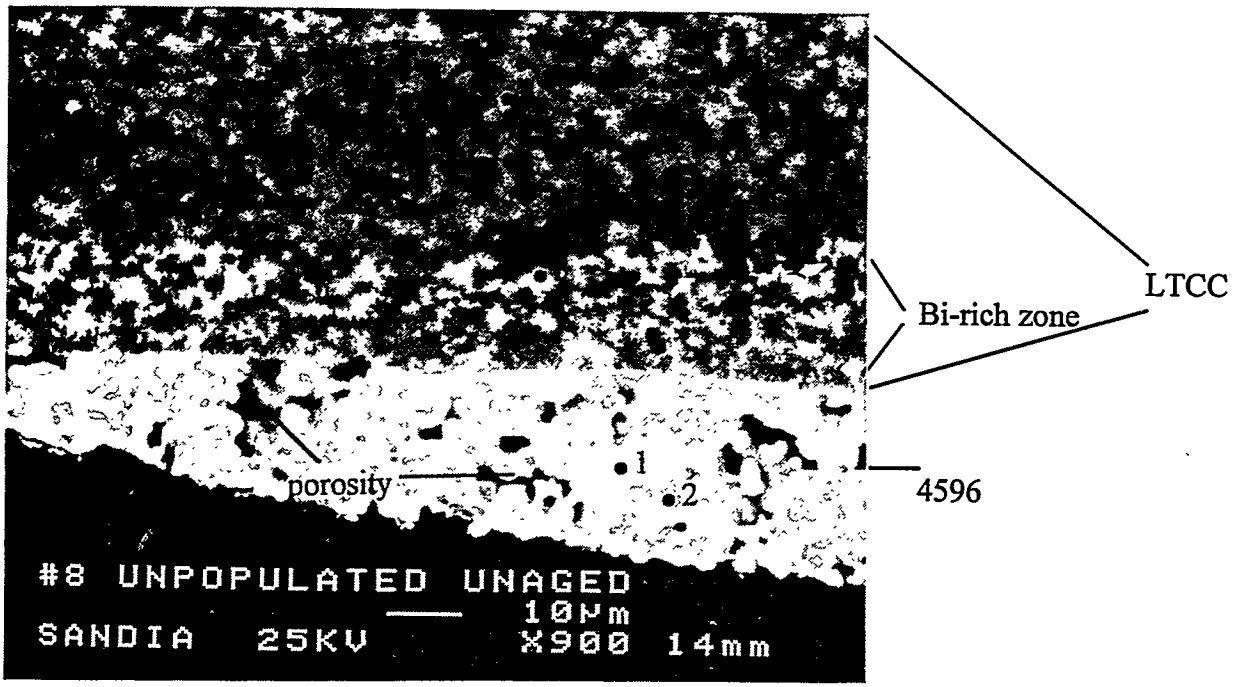

Figure 20B. Higher magnification of boxed area in A shows five locations where EDS spectra were taken. EDS spectra are in Figure 21.

Figure 21 contains EDS spectra of areas identified in Figure 20B.

- EDS spectra of area 1, the brightest phase of the DuPont 4596 layer, contains Au, Pt, and Pd.

- The EDS spectra of area 2, the darker phase in the DuPont 4596, is the glassy phase, which contains all the expected elements Bi, Si, Pb, Al, Ca, Co, and Cd. The EDS spectra of area 2 also contains Au and Pt peaks because the localized areas of the glassy phase are smaller than the analyzed volume.

EDS spectra of areas 3, 4, and 5 show the bulk chemistry of LTCC and the LTCC chemistry near the LTCC/Au-Pt interface. Area 3 is the dark phase of the LTCC containing primarily Al with traces of Si, Ca, and Pb, and area 4 is the lighter phase containing primarily Si, with Al, Pb, Ca, and K. Both of these analyses were taken sufficiently far away from the Au-Pt interface to represent the composition of the monolithic LTCC. The bright band in the LTCC (Figure 20B) is limited to the area between the LTCC and Au-Pt. The brightest phase in that band, area 5, was analyzed and the spectra are shown in Figure 21, area 5. The spectra reveals that glassy constituents from both the LTCC and DuPont 4596 are present, in particular the presence of the large bismuth and lead peaks indicate interaction has occurred between the glass phases of the DuPont 4596 into the LTCC substrate. The thickness of the bismuth-rich layer, 16 to 20 microns, was measured on the front and backside surfaces of the LTCC and no substantial difference was observed. These micrographs and analyses, of the baseline part (TV #8A), show the interaction of some glassy constituents has occurred between the LTCC and DuPont 4596, and that multiple firings and processing to this stage have not caused any segregation of a phase or an isolated layer that would cause a weakened interface.

3.5.5.2 Test Vehicle #8

Test Vehicle #8, a substrate with soldered LCC packages, but unaged, shows the characteristics of the solder/Au-Pt/LTCC interfaces before exposure to the accelerated aging environment. The cross-section of TV #8 was examined and micrographs are shown in Figures 22A, 22B, and 22C. EDS spectra were taken from areas marked on Figure 22C. Again the bismuth-rich band in the LTCC, area 5, occurred only adjacent to the DuPont 4596 and the layer was about 20 microns thick.

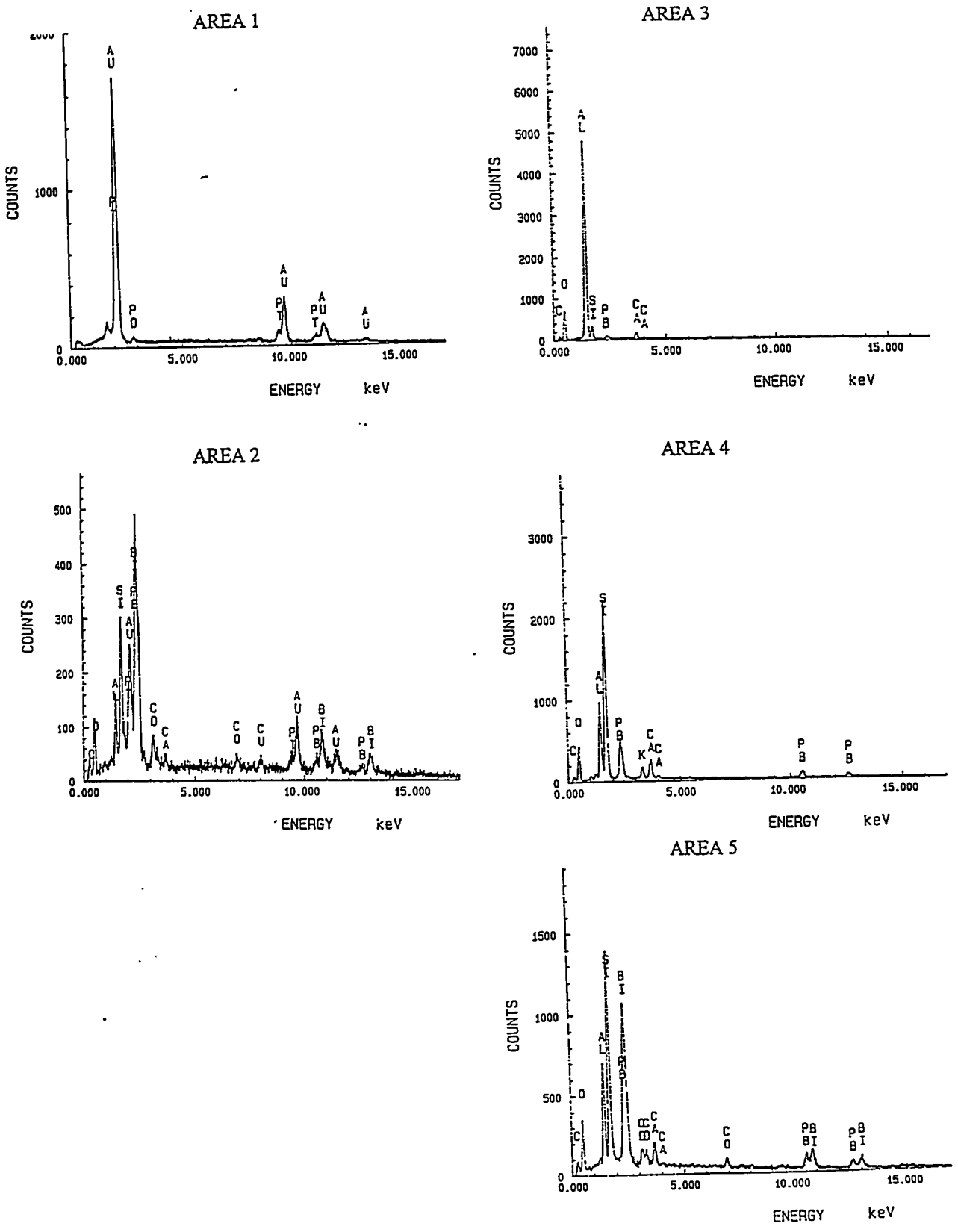

Figure 21. EDS spectra from areas identified in micrographs in Figure 20B from TV#8A.

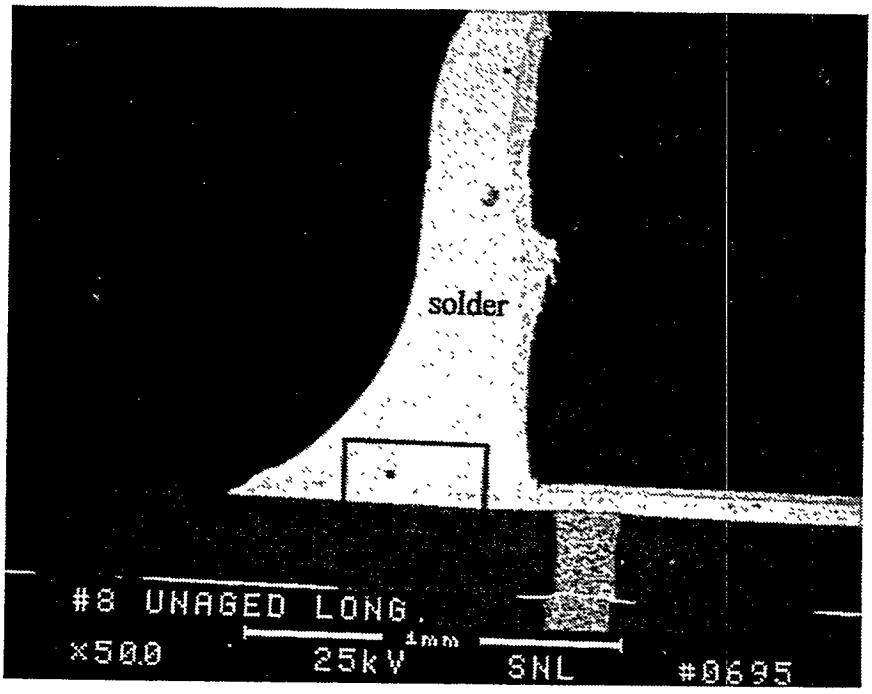

Figure 22A. Low magnification of the solder fillet connecting LCC with LTCC substrate.

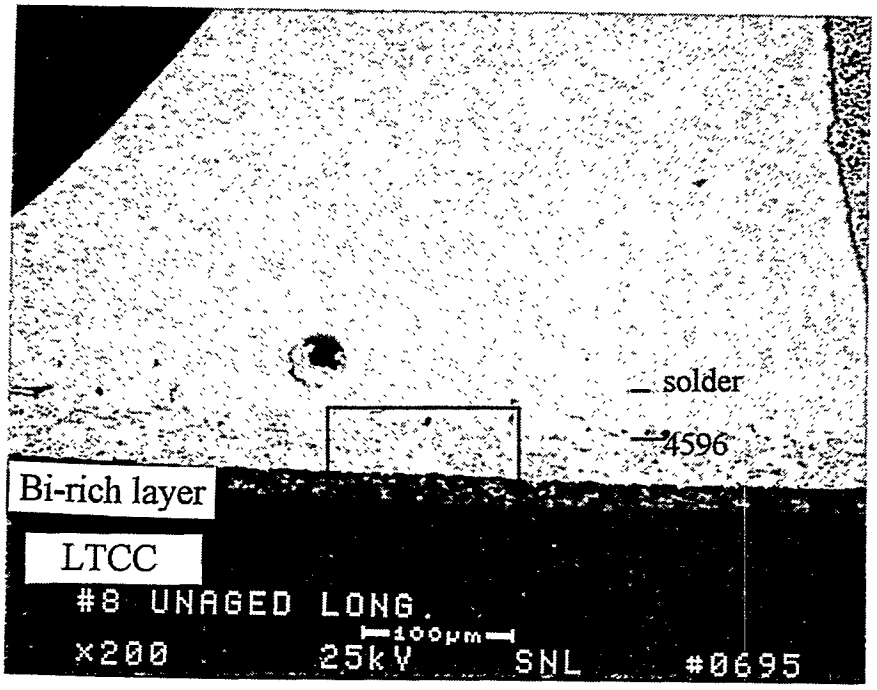

Figure 22B. SEM backscatter image of solder LTCC interface.

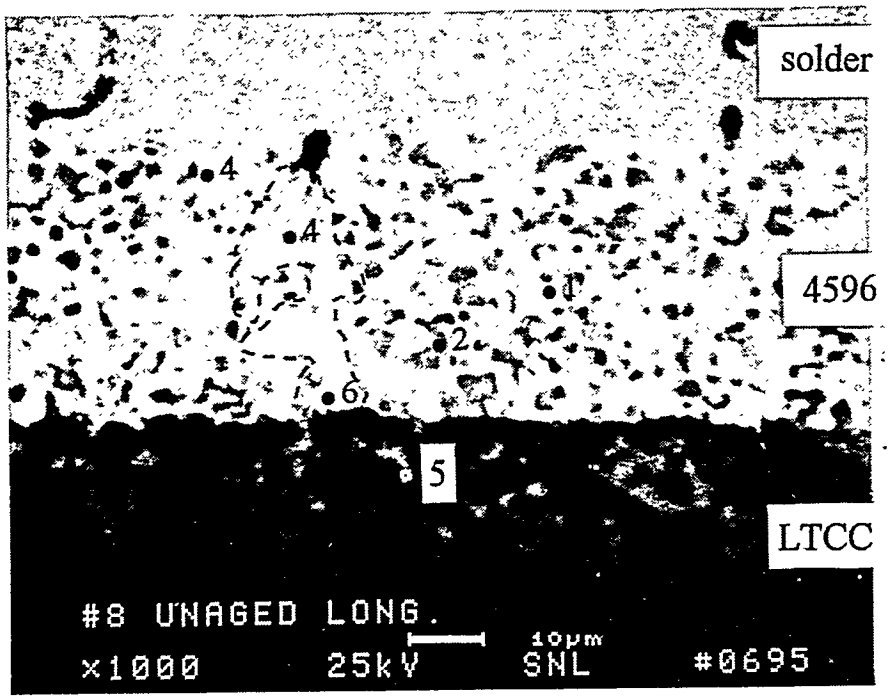

Figure 22C. High magnification of the interface shows solder moving to the LTCC through porosity (6) in the 4596 metallization and development of some intermetallic (4) during the solder process.

Area 2 contains the normal assemblage of elements found in the glassy phase of the DuPont 4596, just as observed in TV #8A, Figure 21, area 2. Area 1, the brightest in the DuPont 4596 layer, contained Au, Pt, and Pd, the same elements found in the unsoldered DuPont 4596 (Figure 21, area 1).

There were two additional distinct phases identified in the Au-Pt layer, areas 4 and 6 of Figure 22C. EDS spectra shown in Figure 23A of area 4, contains Au and Sn, indicating formation of the intermetallic compound. The extent of penetration of this compound, close to the interface, was surprising for a part that had not been aged. Other studies have shown that the Au-Sn intermetallic will form to some degree during the solder reflow process, but it is usually limited to a 1-2 micron thick layer between the solder and Au-Pt metallization.[4]

EDS spectra, shown in Figure 23B, area 6, contains Au, Sn and Pb, indicating that solder physically penetrated into the Au-Pt metallization, in some cases extending to LTCC interface. Because the penetration of the solder was not as a continuous front, this is strong evidence that excessive porosity existed in the DuPont 4596 metallization layer prior to the solder operation.

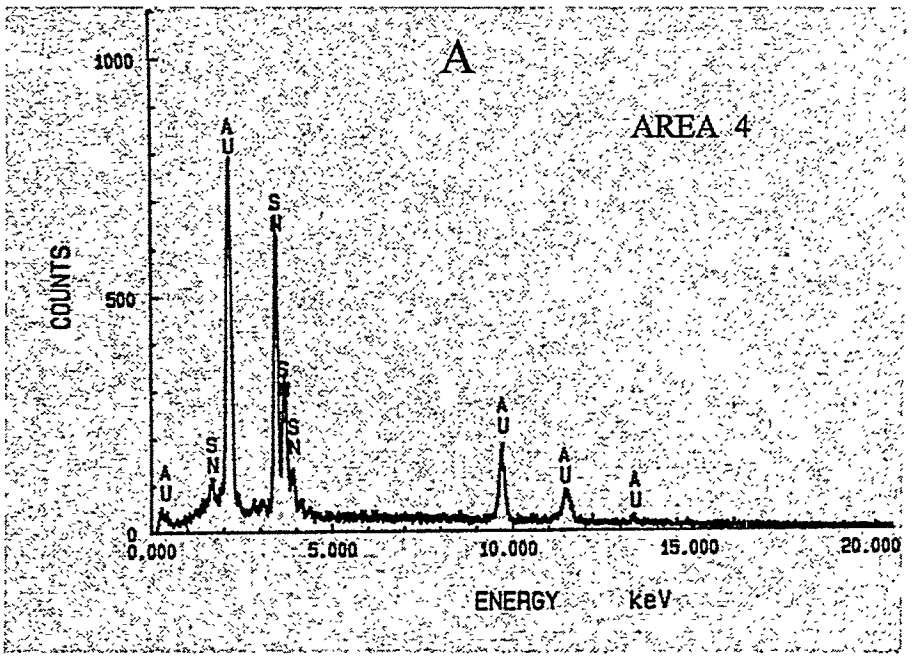

Figure 23A. EDS spectra of intermetallic compound found in the 4596 metallization.

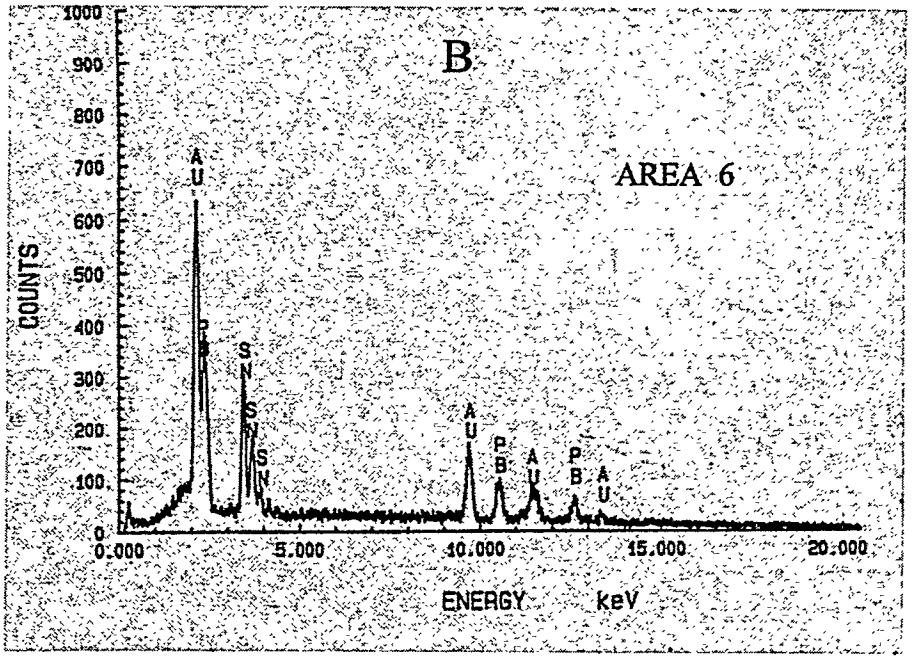

Figure 23B. EDS spectra shows some Pb with the intermetallic, suggesting that the 4596 metallization was sufficiently porous to allow solder to penetrate to the LTCC interface.

3.5.5.3 Test Vehicle #12

Test Vehicle #12, a package that had been processed and environmentally conditioned and tested along with TV #10, but had not failed electrically, was also examined. Cross-sections of TV #12 are shown in Figures 24A, 24B, 24C, and 24D. EDS analysis showed the normal 16- to 20-micron-thick bismuth-rich layer in the LTCC adjacent to the DuPont 4596. This longitudinal cross-section through the toe of the solder pad shows clear evidence that a crack was present in the toe (Figures 24A and 24C) and that there was poor bonding between the solder pads and LTCC, as evidenced by gaps extending along most of the interface (Figure 24B).

The crack in the toe of the solder pad indicates a brittle nature, a typical characteristic of many intermetallic materials. The (*) in Figure 24B marks the only location where bonding, and probably electrical continuity, exists between the LTCC and LCC package. This bonding is limited to the area between the via and some residual overlying Au-Pt metallization.

The micrograph in Figure 24D shows a very different interface microstructure than was observed in the "as-soldered" package (TV #8, Figure 22C). Almost no areas are left of the original Au-Pt metallization in TV #12. The entire layer has been consumed in the development of the 90-micron-thick Au-Sn intermetallic layer. In areas 1 and 3, Figure 24D, EDS analysis confirmed the intermetallic composition and isolated islands of the Au-Pt composition, respectively.

EDS spectra are shown in Figures 25A and 25B. Also, in this micrograph, area 2 Figure 24D, the dark phase, which is distributed throughout the intermetallic, was analyzed. It has the same elemental composition found in the glassy phase of the original DuPont 4596 metallization layer (Figure 21, area 2). This interfacial microstructure shows extensive formation the Au-Sn intermetallic with islands of residual DuPont 4596 glass phase.

3.5.5.4 Test Vehicle #10

The goal of the previous cross-sectional analyses was to develop a microstructure data base from which to compare the electrically failed part, TV #10. In the preparation to encapsulate and cross-section TV #10, the U-2 package popped off the LTCC substrate. The ease with which this separation occurred further indicated that the interface between the LCC solder pads and LTCC substrate was not strongly bonded.

The microstructure of several solder pads were examined on TV #10, specifically the LCC solder pad (pin #6), which had been identified as electrically open during testing. In addition, the microstructure of other solder pads on the U-2 LCC, which were not electrical opens, were examined. Finally, cross-sections of solder pads on two other LCC packages from TV #10 (U-3 and U-9) were examined to check for variability in microstructure.

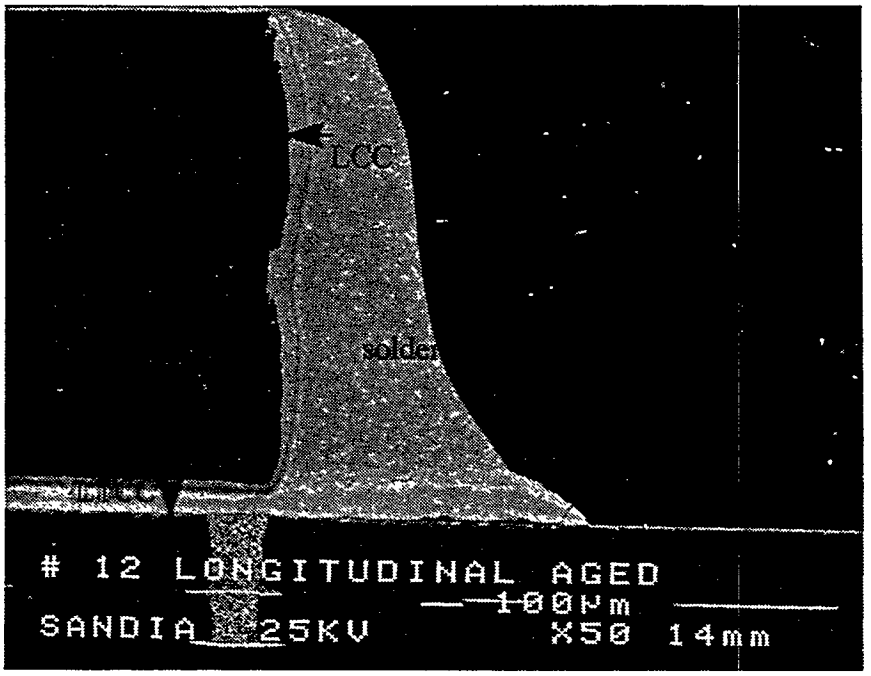

Figure 24A. Crack is evident in toe of solder.

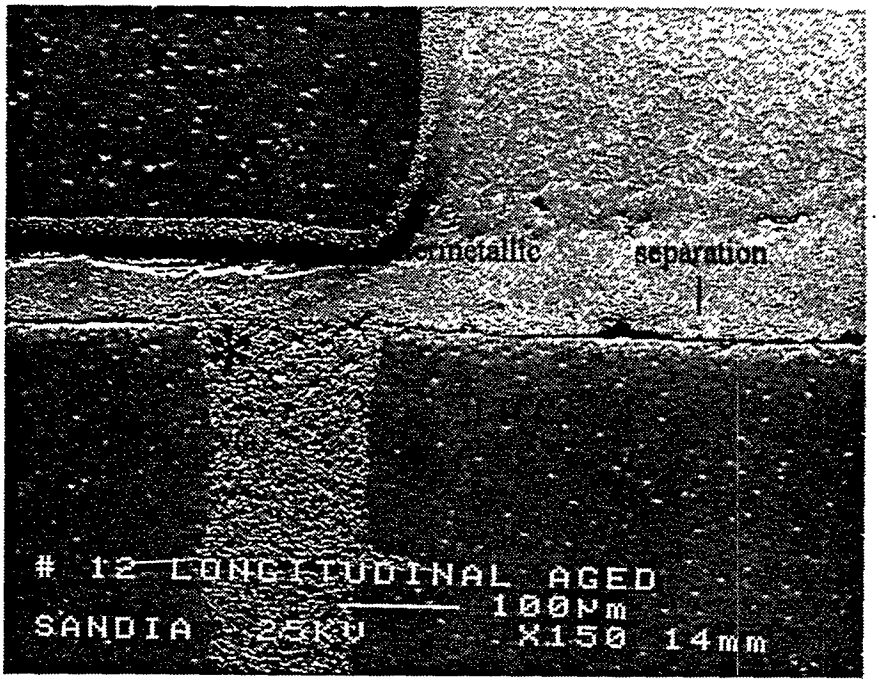

Figure 24B. The only continuity between the LTCC and LCC is through the via (*).

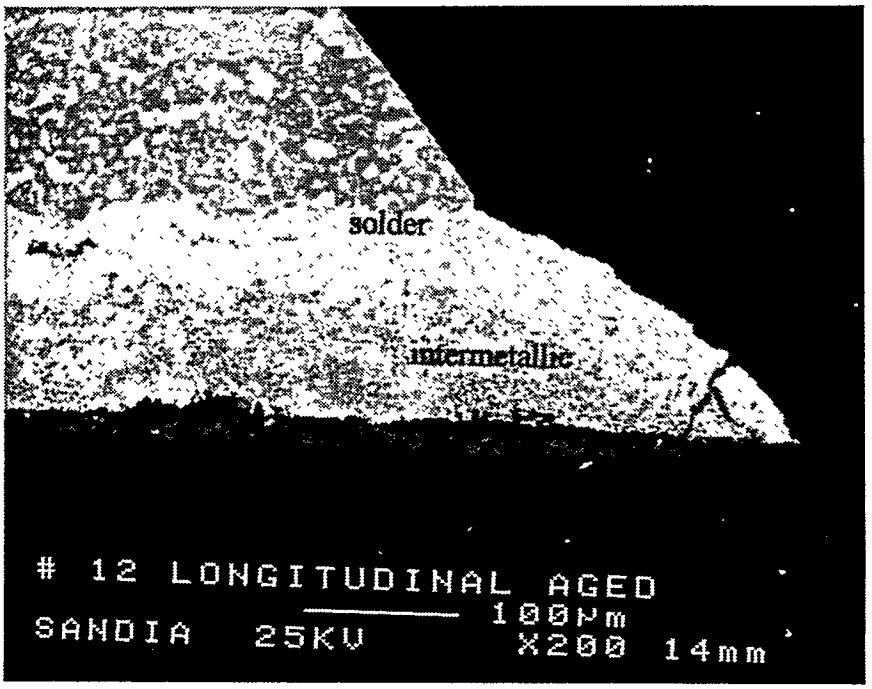

C

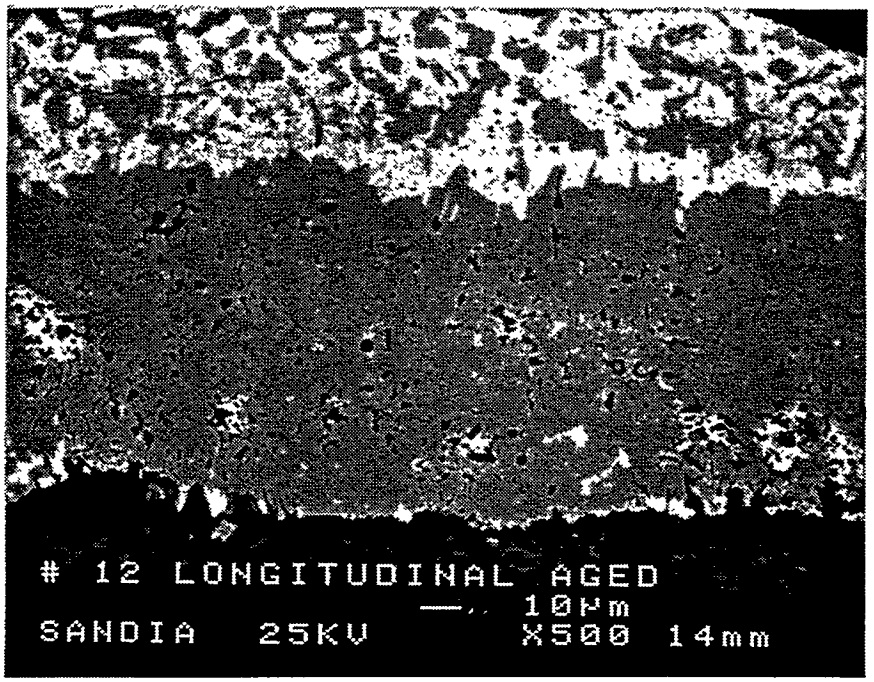

D

Figure 24C and D. Intermetallic has completely consumed the 4596 metallization.

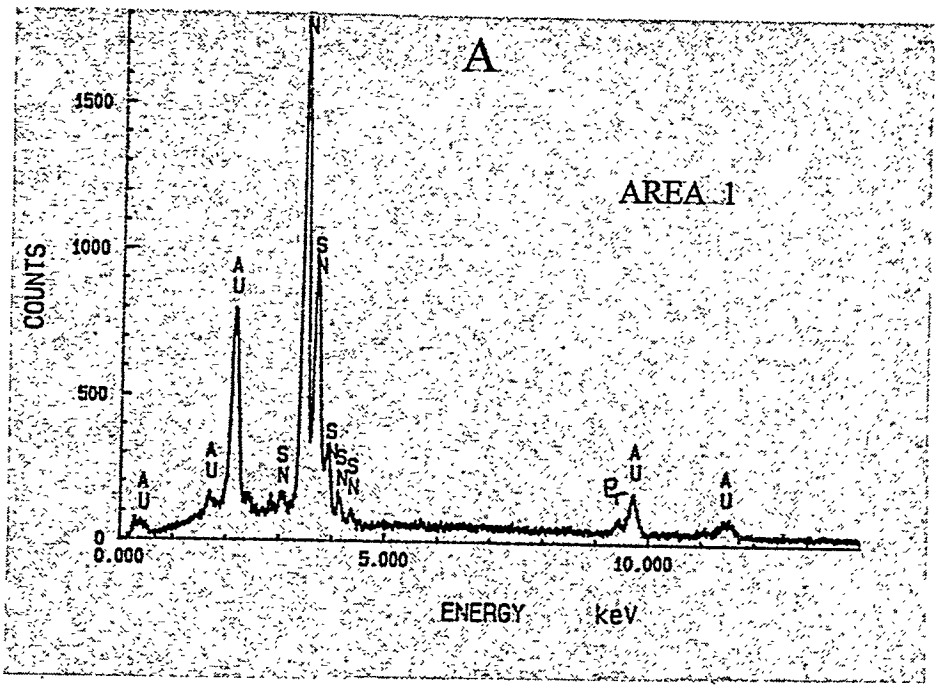

Figure 25A. EDS spectra of intermetallic material developed between the solder and LTCC, its formation consumed most of the 4596 metallization.

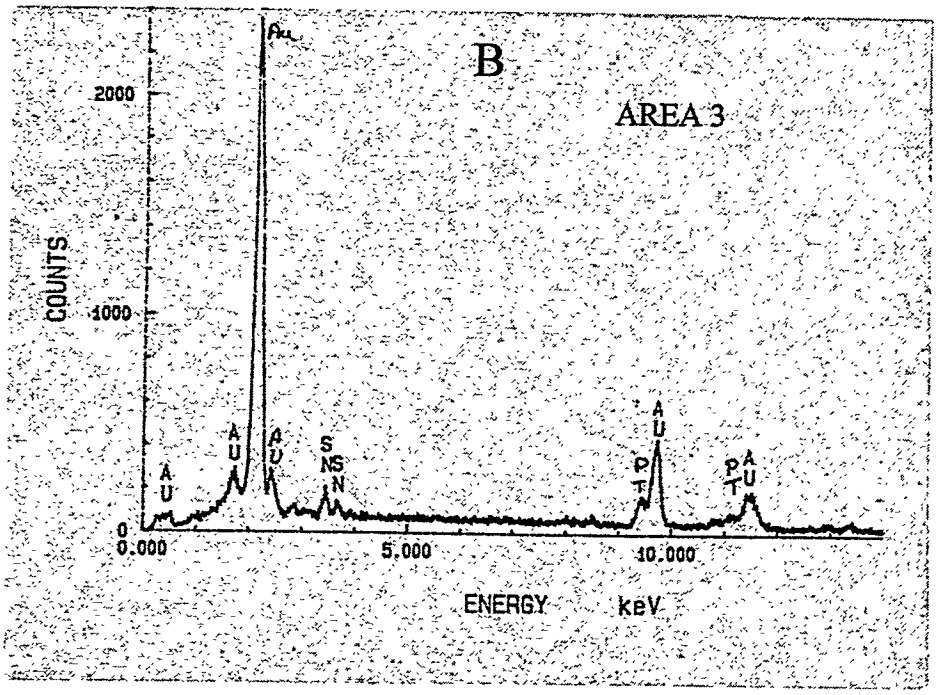

Figure 25B. EDS spectra of the islands of residual 4596 metallization.

Because the U-2 LCC package was so weakly bonded to the substrate, the cross-sections have gaps between the solder pad and LTCC where the epoxy encapsulant penetrated the separation. The microstructures shown in Figures 26A, 26B, 26C, and 26D are typical of all sections examined in TV #10. The 20-micron-thick bismuth-rich layer in the LTCC is present in all sections, as are islands of DuPont 4596 (area 3) remaining at the interface surrounded by the Au/Sn intermetallic (area 1). Isolated areas of the DuPont 4596 glassy phase (area 2) are distributed throughout the intermetallic. EDS spectra of those areas are like the ones in Figure 25, area 1 and 3, and Figure 21, area 2.

The major difference observed in cross-sections of TV #10, as compared with the other test vehicles examined, was in the thickness of the intermetallic layer. The intermetallic layer at pins 4 and 6 of U-2 was not quite as thick as the 90 microns measured in all other cross-sections of aged parts. In pin 4, the intermetallic was only 75 microns thick and in pin 6, the intermetallic was 60 microns thick. All thickness measurements are summarized in Table 9. This thinner intermetallic may indicate some subtle variability in processing such as touch-up or a solder pad or rework of an LCC.

3.5.6 Shear Testing

After the portion of TV #10 had been dropped and the LCC separated from the substrate, the adhesion strength of the LCCs to the LTCC substrates came under suspicion. The adhesion strength of several components to the LTCC substrate on each of the test vehicles TV #8, TV #10, and TV #24 was measured. A standard test is not available to measure the adhesion strength of the LCCs or thick film metallization at this point. A shear test was developed for the purpose of comparing the adhesion strength and failure modes of the three available test vehicles. Three different types (sizes) of LCCs were available on each test vehicle.

A shear test was developed in which the test vehicles were held vertically in a vise-like clamp. A shear tool was designed and fabricated to apply a uniform load to the bottom side of an LCC soldered to the test vehicle. An Instron Materials Test System was used to apply a shear load to the LCC as the shear tool was moved in an upward direction. Data obtained from the shear tests are summarized in Table 10.

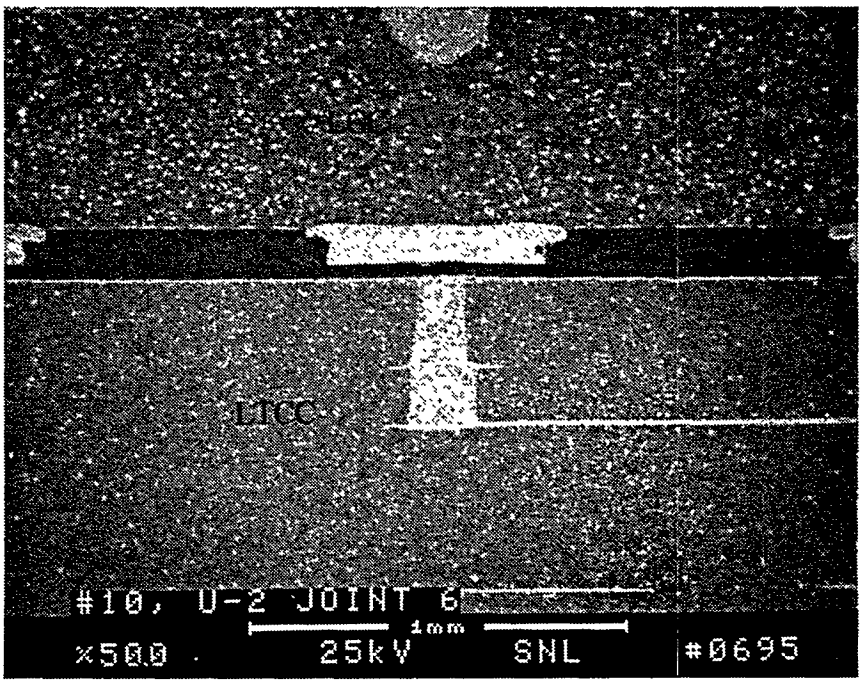

A

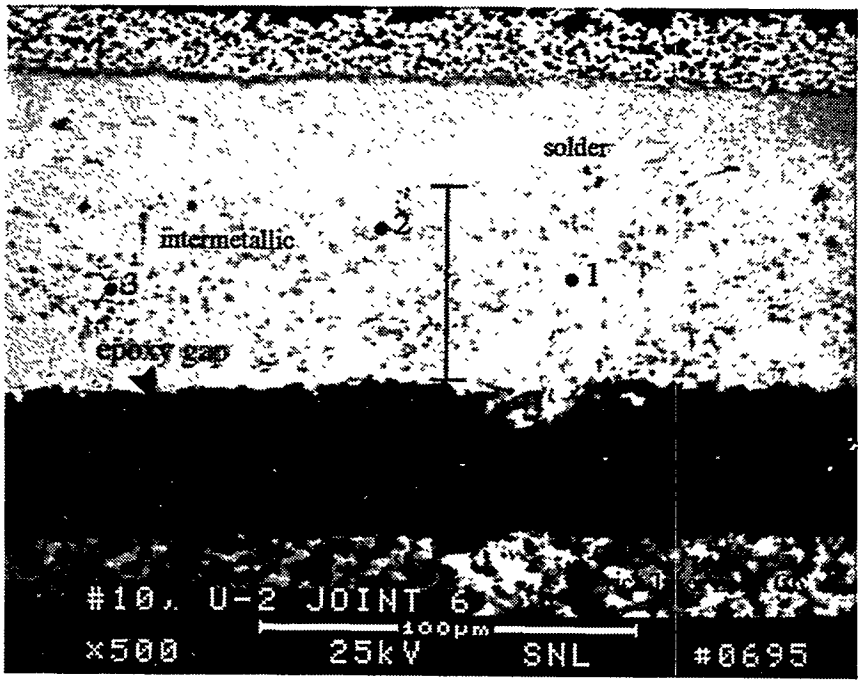

B

Figure 26A and B. TV#10, LCC package U-2. A and B are micrographs of pin 6 where the electrical open was observed.

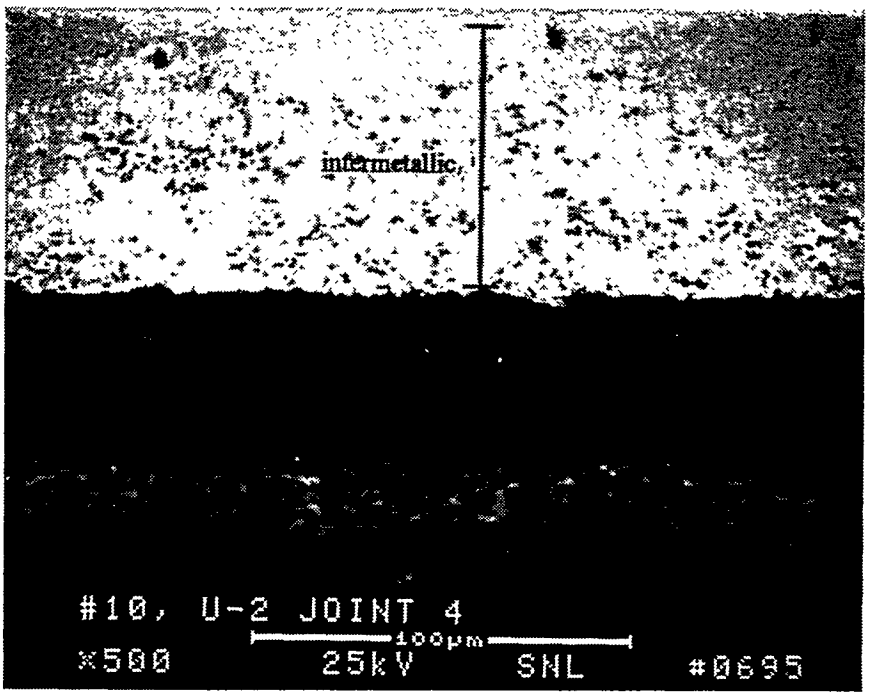

C

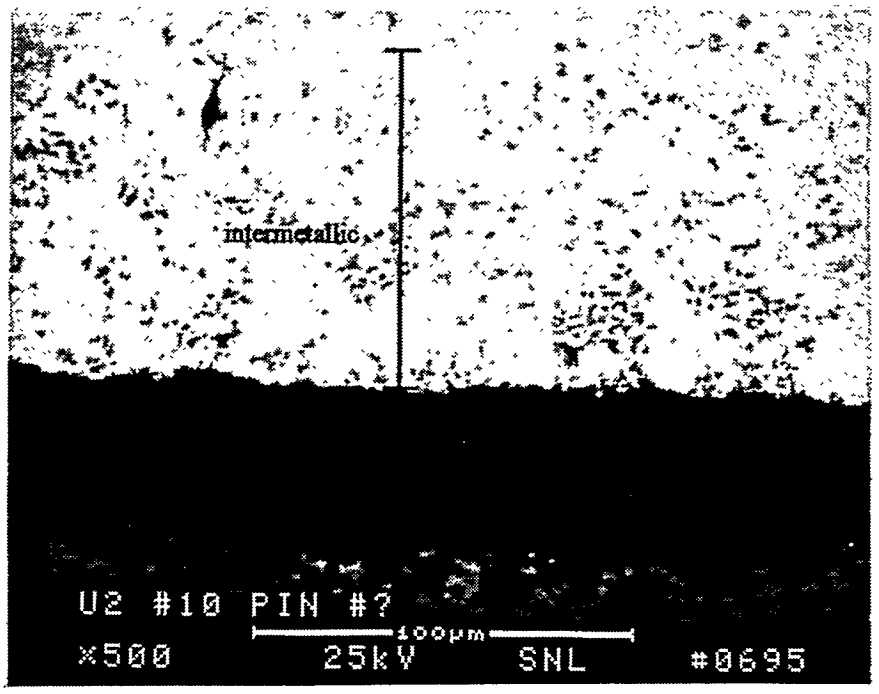

D

Figure 26C and D. C and D are cross-sections of two other pins on U-2 shows thickness of the intermetallic.

Table 10. LCC Shear Test Data.

LCC ID	# OF JOINTS	LOAD TO FAILURE (LB.)		
		TV #10	TV #12	TV # 24
U-4	16	36	28	49
U-3	32	20	26	63
U-7	40	45	55	no test

TV #10: Aged; showed electrical open; all joints failed at the substrate except three joints of U-4 failed in solder.

TV #12: Aged; no electrical failures; all joints failed at the substrate except one joint of U-4 failed in solder.

TV #24: Not aged; U-4 all joints failed in solder; substrate cracked when attempting to shear off U-3.

With the limited number of samples available for testing, these results do not incorporate a high confidence level; however, they do allow a first order comparison between aged and unaged test vehicles. The unaged test vehicle, TV # 24, had higher shear strengths than the two aged test vehicles, TV #10 and TV #12. In fact, the substrate of TV #24 was broken when trying to shear off U3. The load was 63 pounds when the substrate cracked and this prevented U7 of TV #24 from being tested.

Probably of more significance is the comparison of the failure modes of the aged and unaged samples. The aged test vehicles failed at the interface between the LTCC substrate and thick film metal/intermetallic surface (see Figure 27) while the unaged test vehicles failed within the solder. This provides a good indication that the two aged test vehicles had reached their limit of time and temperature exposure, and that the majority of the thick film metal had reacted with the solder to form intermetallic compound at the LTCC substrate. Even though electrical failures occurred only on TV #10, it is a safe assumption that TV #12 could have failed at any time, as shown by the limited amount of bonding observed in Figure 24B and the low shear failure loads.

3.5.7 Conclusions

Evaluation of the various test vehicles allowed us to examine whether there are significant differences in the microstructure/composition of the LTCC/DuPont 4596 interface as a function of processing and aging. No evidence was found to indicate that multiple firing steps changed the thickness of the DuPont 4596 metallization or created a segregated glassy layer. Also, there was no indication of any fracture within the LTCC substrate that would have interrupted the electrical function.

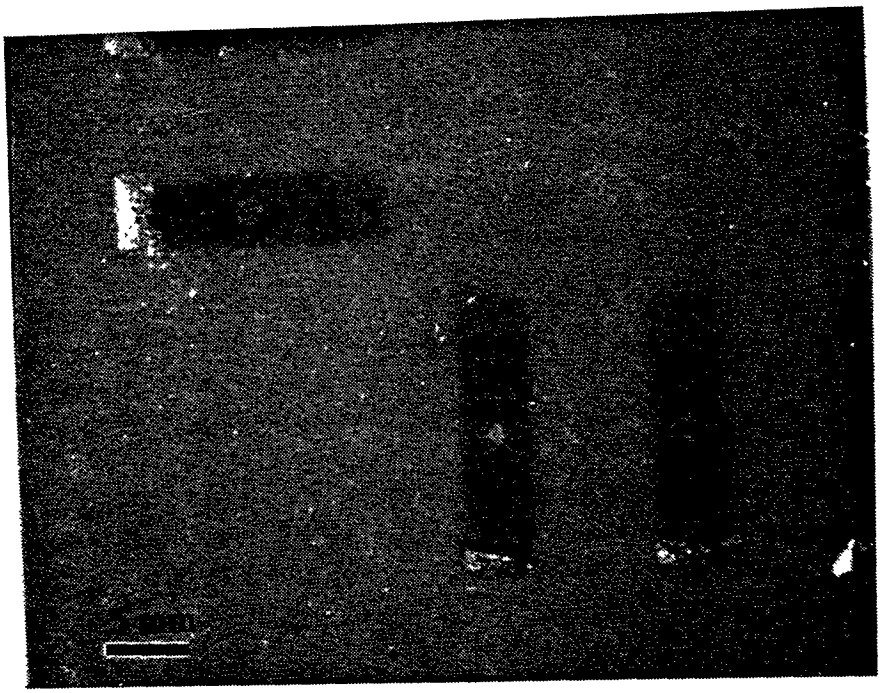

Figure 27. Low magnification view of failed pads on TV#12. These pads failed during shear testing at the interface between the LTCC and metallization. The appearance is very similar to the TV#10 sample which failed when accidentally dropped. Compare with Figure 17.

However, we found ample evidence of a Au/Sn intermetallic compound forming between the LTCC and soldered LCC (TV #10 and TV #12) that had been temperature aged. This intermetallic had completely consumed the DuPont 4596 metallization layer. Intermetallics are known to be brittle in nature, may introduce stress at a joint, and potentially lead to interface separation. Compositional analysis of separated surfaces indicates the possibility of Sn migration not only from the top (vertical migration) surface but also from the edges (lateral migration) of the LCC solder pads. The difference in thermal expansion coefficients between the LTCC substrate and the intermetallic compound may have contributed to the fractured interface. These fracture surfaces were identified as the root cause of the electrical opens in TV #10.

It is important to note that the DuPont 4596 metallization layer was quite porous, as observed in both the unsoldered/unaged and "as soldered" part, allowing penetration of solder to the LTCC interface. The only significant difference observed between aged parts was in the thickness of the intermetallic layer, which was thinner at pins where electrical opens had been observed. Nominal metallization fired thickness for double-printed DuPont 4595 is approximately 1.5 mils.

It should be mentioned that the test vehicles that exhibited the electrical failures were aged at 125°C for 1000 hours — a dramatic overtest as compared with the anticipated storage environments during life of program. More realistic estimates of temperature conditions results in exposure of the MET to a maximum of 75°C for less

than 25% of the expected stockpile life. The intermetallic growth model developed by Stephens, et. al.[4] for this solder-metallization system predicts an intermetallic compound thickness of 1.5 mils when exposed to 75°C for 30 years.

Theoretically, the percentage contribution of DuPont 4596 metallization to the formation of the intermetallic compound is less than 50 percent. This equates to less than 0.7 mils of the metallization being consumed by the solder. This calculation does not take into account porosity of the metallization, which can contribute to the formation and the rate at which the intermetallic develops at the substrate-conductor interface. The porosity in the metallization might explain the variability observed in the intermetallic compound thickness of aged samples. In addition, variability in processing, such as "touch-up" of a solder pad or rework/replacement of the LCC, could contribute to variations in intermetallic thickness.

3.5.8 Recommendations

In an effort to slow down the complete consumption of the DuPont 4596 Au-Pt metallization and subsequent formation of an intermetallic compound at the LTCC interface, changes were incorporated in the LCC solder pad design. The top Au-Pt metallization layer was changed from double print to triple print. This should increase the metallization thickness from 30 microns to 40 microns. In addition, the incorporation of a dielectric screen printed window frame around the solder pad will eliminate "lateral" migration of the Sn. These two design changes will (1) provide sufficient Au-Pt metallization that will not be consumed by the intermetallic growth, and (2) reduce and/or eliminate the lateral migration of the intermetallic compound. The purpose of the design changes is aimed at providing a reliable microstructure interface for stockpile storage.

Another critical area that is presently being addressed pertains to the solder assembly operation. The number of times the LTCC assembly is subjected to reflow operations, whether as part of the standard assembly process or as a result of rework, will affect the thickness of the intermetallic. Performance of the selected pad geometry/design to multiple reflow operations, as well as rework or touch-up, needs to be characterized on the basis of intermetallic growth. This information will serve to better define and control the solder assembly process, thereby improving the quality and reliability of the product.

Finally, the issue of porosity of the DuPont 4596 and its effects on intermetallic growth needs to be better understood. The fact that porosity of a fired thick film conductor is affected, in some way, as a result of firing profile parameters is not new, however its importance has been underrated. A thorough understanding of this behavior would increase the long term/stockpile reliability of soldered assemblies.

4. Summary and Recommendations

This report confirms the susceptibility of LTCC substrates, fabricated using DuPont 951 "Green Tape"™, to slow crack growth. Through testing of coupons, representative of the MET design, a minimum stress threshold for slow crack growth to occur of 6.5 Kpsi was established. Finite element analysis was used to optimize the MET substrate thickness and mechanical support design to ascertain that applied loads would not induce stress levels above the slow crack growth threshold. Validation of the formulated predictive stress model by testing was performed at ASFM&T.

Fractographic analysis of units that failed mechanically revealed large flaws in the substrate at the origins of crack propagation. There was no evidence to indicate that these flaws were characteristic of the MET LTCC design or of the LTCC fabrication processes. In most cases, failures are attributed to the accumulated exposure of samples to varying levels of shock. Subsequent testing of samples with increased substrate thickness and an improved mechanical support scheme showed failure would occur only at shock levels substantially above product specification requirements.

Failure analysis performed on the unit that failed continuity test after exposure to random vibration can be attributed to the dissolution of the gold-platinum alloy conductor by the tin-lead solder. Changes to the solder pad configuration were incorporated to reduce or eliminate the solder-metallization intermetallic from reaching the interface during MET stockpile lifetime.

Testing via four-point bend bars demonstrated that the laser approach for sizing LTCC substrates induced flaws, which reduced the overall strength of test samples as compared to diamond saw-cut samples. Laser-scribed samples were processed at settings typical of those used to process alumina substrates. Parametric characterization of the laser process may yield an optimized set of conditions that could improve the mechanical performance of scribed samples. However until this is done, the diamond-saw process should remain as the only approved methodology for sizing MET LTCC substrates.

The qualification of Low Temperature Cofire Ceramic as a viable network technology for WR electronic assemblies using surface-mount component attachment was driven by the MCCS Encryption Translator (MET) requirements. The performance of the LTCC networks tested under this qualification program were premised on the MET design and evaluated against metrics that were derived from the MET electrical, mechanical, and environmental requirements. Due to time constraints imposed by MET program

schedules and limitations in the available funding for technology characterization/development, an extensive evaluation of LTCC technology for use outside the boundaries as defined by the MET was not possible. The results from this Qualification Program may be considered as a starting point, but not as comprehensive design criteria for other applications and/or designs.

Despite the perceived maturity of LTCC, this technology is still under development, in particular where nuclear weapons reliability performance is a requirement. The capabilities and potential advantages of LTCC technology for realization of high-density complex electronic modules are numerous and should continue to be explored by Sandia National Laboratories and DOE.

5. References

1. R. W. Davidge, *Mechanical Behavior of Ceramics.* Cambridge University Press, 1986, p.140.

2. ASTM Designation C 1161-90, *Annual Book of ASTM Standards*, Vol. 15.01, 1991.

3. George Quinn, "Strength and Proof Testing," *Glass and Ceramics*, Vol. 4, ASM International, 1991, p. 585.

4. Memo from J. J. Stephens, 1832 and P. T. Vianco, 1831 to T. J. Ferguson, 2341 and J. A. Vinson, AS/KCD, D/851, "Solid State Reaction Kinetics of the 4596 Thick Film/63Sn-37Pb Solder System: Analysis of Aging Experiments," April 1, 1993.

Distribution

6 Allied Signal Inc.
FM&T/KC
Attn: Howard Morgenstern, ER2-2
Tom Tarbutton, ER5
John Bosnack, ER5
Larry Zawicki, ER2-2
Stacey Landers, ER5
Greg Barner, ER2-2
2000 E. 95th Street
Kansas City, MO 64131-3095

2	MS 0311	Ken Kimball, 2671
1	0333	Jill Glass, 1833
3	0367	Saundra Monroe, 1833
1	0367	John Stephens, 1833
3	0443	Steven Burchett, 9117
1	0447	Rich Kreutzfeld, 2111
1	0486	Stan Kawka, 2123
2	0487	J. F. Nagel, 2121
1	0537	Ray Thomas, 2314
1	0637	Ray Sanchez, 12336
3	0959	Steve Garrett, 1471
3	0959	Fernando Uribe, 1471
1	0959	Bob Poole, 1471
1	1073	Bill Conley, 1277
1	0367	Brian Damkroger, 1833
1	1411	Paul Vianco, 1833
1	9106	Robert Oetken, 8417
1	9106	Gary Simpson, 8417
1	9018	Central Technical Files, 8940-2
5	0899	Technical Library, 4414
2	0619	Review & Approval Desk, 12690 For DOE/OSTI